Physics – Uspekhi **46** (10) 1053 – 1075 (2003)

REVIEWS OF TOPICAL PROBLEMS PACS numbers: 07.85.Fv, **41.50.+h**, **42.25.–p**

Channeling of neutral particles in micro- and nanocapillaries

S B Dabagov

DOI: 10.1070/PU2003v046n10ABEH001639

Contents

Abstract. After a brief review of the main areas of research in X-ray optics and an analysis of the development of capillary optics, a general theory of radiation propagation through capillary structures is described in both geometrical optics and wave optics approximations. Analysis of the radiation field structure inside a capillary waveguide shows that wave propagation in channels can be of a purely modal nature, with the transmitted energy mostly concentrated in the immediate neighborhood of the capillary inner walls. A qualitative change in radiation scattering with decreasing channel diameter — namely, the transition from surface channeling in microcapillaries to bulk channeling in nanocapillaries — is discussed.

1. Introduction

For more than a century scientists all over the world have dealt with X-rays discovered in 1895 by the German physicist W K Röntgen [1, 2]. At present the interaction of X-ray radiation and matter lies at the base of many methods of not only physics but also biology, medicine, materials science, microscopy, X-ray testing, etc. In addition to the common X-ray tubes, the main sources of X-ray radiation are synchrotrons, storage rings equipped with undulators and wigglers, and micropinch and laser-plasma sources [3 – 6].

S B Dabagov P N Lebedev Physics Institute, Russian Academy of Sciences
Leninskiĭ prosp. 53, 119991 Moscow, Russian Federation
INFN — Laboratori Nazionali di Frascati, Frascati, Italy
Tel. (39) 06 9403 2877. E-mail: dabagov@lnf.infn.it

Received 14 May 2003
Uspekhi Fizicheskikh Nauk **173** (10) 1083 – 1106 (2003)
Translated by E Yankovsky; edited by S N Gorin

Two very important discoveries made before the wide use of X-ray radiation were the diffraction of X-rays, which was discovered by Laue's group [7], and Compton's pioneering work [8] (1923) on the reflection of X-rays from a smooth surface. The former made it possible to control X-rays and to produce coherent monochromatic and collimated beams; the latter showed that X-rays are shortwave electromagnetic waves. This idea made it possible to use the principles of ordinary light optics in the X-ray range. The first results of studies devoted to the analysis of the optics of grazing incidence of X-rays were published in 1929 [9].

Since in ordinary crystals the interplanar spacing does not exceed 4 – 5 Å, the Bragg condition $2d\sin\theta = n\lambda$ (d is the interplanar spacing, θ is the glancing angle, λ is the wavelength of the radiation, and n is the diffraction order) with $n = 1$ suggests that there is a limit in the use of crystals as X-ray optical elements when $\lambda < 10$ Å. At longer wavelengths the common practice was to use grazing-incidence optics, which was considered the most effective way of controlling beams of X-ray radiation. Note that all the X-ray optical systems were actually based on two schemes of grazing incidence, one proposed in 1948 by Kirkpatrik and Baez [10], and the other proposed in 1952 by Wolter [11]. Both schemes require very precise coincidence of the optical axes of the lenses and a thorough treatment of the surfaces.

In the last two decades the situation has changed dramatically thanks to progress in perfecting the method of ultrasmooth-surface treatment, which has made it possible to substantially broaden the possibilities of common grazing-incidence optics. Furthermore, because of the development of thin-film deposition technology and methods of microlithography, two new classes of X-ray optical elements have been produced, namely, multilayer interference mirrors and diffraction zone plates [12 – 16]. What deserves special

mention is the appearance of entirely new X-ray optical systems consisting of capillaries [17, 18]. Capillary X-ray optics is the optics of multiple reflection. It differs favorably from the existing X-ray optical systems in such parameters as the aperture, the effectiveness of radiation bending through large angles, the increase in the concentration of X-ray radiation in the focal spot, and others.

At present there is intensive research in all areas of X-ray optics. X-ray optical elements are used in new high-power X-ray sources and to perfect devices used in transmission of X-ray images, in elemental analysis, in diffraction, etc. The number of scientific publications (journals, monographs, and collections of articles on the subject) is constantly growing, and so is the number of publications associated with problems of controlling beams of X-ray photons and neutral particles. Every year new conferences and workshops devoted to X-ray optics and its applications are held. In short, the present period of intense development of optics of the X-ray range may be called the 'renaissance of X-ray optics' [19].

2. X-ray optics

Below we discuss the main principles of X-ray optics.

The optical properties of matter in the X-ray range of the spectrum, which determine the complexity of dealing with X-ray radiation, are expressed by the following model of the dielectric constant of matter:

$$\varepsilon = 1 - \delta + \mathrm{i}\beta\,, \tag{1}$$

with $\delta, \beta \ll 1$. From the data on optical constants (see Ref. [20]) it immediately follows that the index of refraction of any material, $n \equiv \sqrt{\varepsilon}$, is, for all practical purposes, equal to unity. Hence, it is difficult to use elements of common refraction optics in this wavelength range. It also turns out that it is impossible to use reflecting mirrors of normal incidence, with the exception of cases of multilayer optics. Indeed, the coefficient of reflection of an electromagnetic wave from a planar surface, $R(\theta)$ (here θ is the glancing angle between the incident beam and the surface), is determined by the Fresnel formulas for s and p polarizations [21]

$$R_{\left\{{}^{s}_{p}\right\}}(\theta) = \left| \frac{\left\{{}^{1}_{\varepsilon}\right\} \sin\theta - (\varepsilon - \cos^2\theta)^{1/2}}{\left\{{}^{1}_{\varepsilon}\right\} \sin\theta + (\varepsilon - \cos^2\theta)^{1/2}} \right|^2 , \tag{2}$$

which means that when the incidence of the X-ray wave is normal, or $\theta \simeq \pi/2$ (the optical density of the substance is low), we have, irrespective of polarization, the simple approximation

$$R\left(\frac{\pi}{2}\right) \simeq \frac{\delta^2 + \beta^2}{16}\,. \tag{3}$$

According to this formula, when δ and β are small (and this is the case for practically all substances), the reflection coefficient is negligible.

The optical elements of the X-ray range can be broken down into four groups, depending on the principle of operation [22, 23]:

(1) grazing-incidence optical elements based on the phenomenon of total external reflection (TER);

(2) multilayer interference mirrors of normal incidence;

(3) transmission diffraction elements (zone plates and gratings);

(4) refraction X-ray lenses of normal incidence.

X-ray optical systems of grazing incidence are based on the TER phenomenon, which is caused by the fact that the dielectric constant of almost all materials is smaller than unity in the X-ray range since $\delta > 0$, i.e., the vacuum in this region of the spectrum is more optically dense than matter. Hence, if absorption is taken into account, the reflection coefficient is close to unity, provided that the glancing angle θ does not exceed the critical TER angle $\theta_c \simeq \sqrt{\delta}$ or the Fresnel angle (see Ref. [24]).

Since in grazing-incidence optics we deal with very small angles ($\theta \ll 1$), strict requirements concerning the treatment of the reflecting surface become obvious. The problem of the influence of surface roughness on the parameters of the reflected beam is very important in X-ray optics [25]. For typical grazing angles $\theta \simeq \theta_c/2$, the height of the roughnesses should not exceed, as a rule, 10 – 20 Å.

It must also be noted that aberrations in optical systems are very large in the case of grazing incidence. Hence, to achieve satisfactory resolution of the devices that transmit X-ray images, the quality of the reflecting surface must be close to ideal. Moreover, small grazing angles dramatically limit the aperture ratio of grazing-incidence devices.

Despite the existing technical problems, grazing-incidence optics remains one of the most promising areas of research, since only such X-ray optical elements make it possible to produce beams of X-ray radiation within a fairly broad spectral region.

Lately, a new area in grazing-incidence optics has received much attention — that of multiple-reflection optics. New X-ray optical systems make it possible to turn X-ray beams by large angles and effectively concentrate and collimate beams as compared to the ordinary elements based on single and double reflections [17].

Another area of X-ray optics that is being actively researched is multilayer X-ray optics, whose operation is based on interference reflection of X-rays from multilayer coatings [26]. Multilayer interference structures consist of alternating substances that have different dielectric constants, with the effective period of the structure equaling $\lambda/2$. The maximum coefficient of reflection of X-rays from the multilayer interference structure can be attained by partitioning the period between the layers in an optimal way. Obviously, irrespective of how well the layer thicknesses are optimized, the coefficient R of reflection of an X-ray wave from one interface is very small. For the reflection coefficients to be large, the structures must consist of a large number of layers, $N \propto R^{-1/2}$ (since the waves reflected by the interfaces add up in the phase). Moreover, Bragg conditions must be met if effective interference of the reflected waves is to be achieved. All this suggests that there is a need to fabricate ultrathin continuous films with a thickness of several atomic monolayers. Of course, the fact that such layers must be very thin complicates the fabrication of multilayer interference structures.

Note that a very important feature of multilayer interference X-ray optics is the normal incidence of radiation on the reflecting surfaces. This considerably simplifies the choice of the proper shape of the reflecting surfaces and substantially reduces aberration because of the transition to paraxial optics.

Another class of X-ray optical elements must also be mentioned: zone plates and diffraction gratings. Their principle of operation differs in no way from that of optical elements of the visible range [4, 27]. Resolution in diffraction structures directly depends on the width of the individual

elements of the structure so that, on the one hand, one must reduce the width of these elements as much as possible and, on the other, the elements must be sufficiently thick so as not to transmit radiation in the opaque sections. Fabrication of structures with elements whose thickness-to-width ratio is of order 10 or higher constitutes a complex technical problem. In addition, zone plates have a very low output power (the fraction of the radiation concentrated at the central maximum does not even theoretically exceed 10%). Despite all these difficulties, it must be noted that, for example, X-ray microscopes with zone plates as focusing elements have the highest spatial resolution achievable today.

During recent years extensive research has been in progress in the field of the development and application of refractive normal-incidence X-ray lenses [28 – 31]. Such optics consists of a system of cylindrical or spherical openings of a certain diameter arranged one after another along the path of propagation of the X-ray radiation, each opening acting as a refracting lens. A set of such lenses significantly reduces the focal distance and increases the aperture of the device. Despite the fact that the optical properties of materials in the X-ray range suggest the strong absorption of radiation, the refracting optics developed in Refs [28 – 31] has proved its high effectiveness in producing microfocal sources of X-ray radiation.

3. Capillary multiple-reflection optics

Many problems (such as the bending of a ray of polychromatic radiation through large angles and the increase in the radiation flux impinging on a target, to name some) require that we have control of the beams of radiation within a broad frequency range. Obviously, this problem can be solved quite effectively by using grazing-incidence optics. Ordinary optical systems [32 – 34] have proven ineffective due to their low power. Since a single reflection may 'turn' an X-ray beam only through an angle $2\theta_c$, only beams that leave the source at small angles ($\leqslant \theta_c$) to the optical axis of the system can be focused on the target: the grazing-incidence focusing system with one or two reflections accumulates on the target only a very small ($\propto \theta_c^2$) fraction of the radiation emitted by the source.

New possibilities in controlling beams of broadband radiation have emerged as a result of using elements of multiple-reflection X-ray optics of grazing incidence [35]. The possibility of controlling X-ray beams via multiple reflection in hollow tubes has been known for a long time [36 – 42]. Only later did Kumakhov [43, 44] suggested using a system of capillaries packed in a certain way for the formation of X-ray beams with specified parameters.

3.1 A capillary as an element of X-ray optics

Let us consider the bending of an X-ray beam by a curved surface with a dielectric constant ε. Suppose that the beam impinges on the surface at a small angle $\theta \leqslant \theta_c$, where

$$\theta_c = \frac{\omega_0}{\omega} \tag{4}$$

is the critical TER angle, with ω_0 being the plasma frequency of the surface's material (30 eV is a typical value of the plasmon energy for the glass materials), and ω the frequency of the X-ray radiation. Then, in view of multiple reflections the beam will be 'turned' through an angle ϕ, the opening angular span of the reflecting surface (Fig. 1a). When the grazing angles are very small, the coefficient (2) of a single reflection can be approximated as follows:

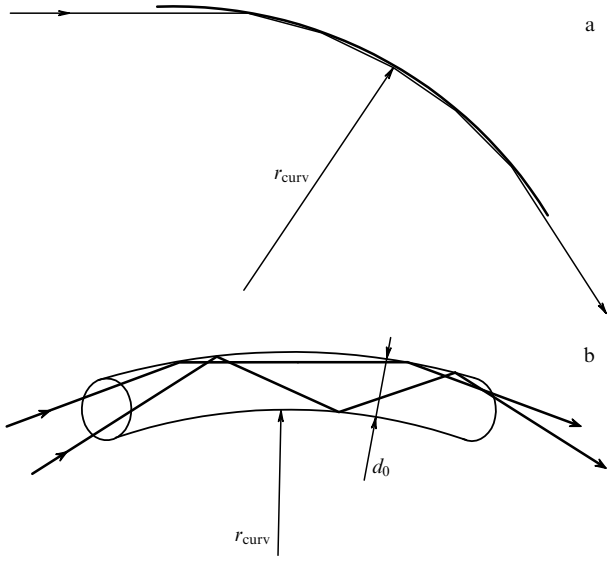

Figure 1. The bending of a beam by a curved surface with a curvature radius r_{curv} (a) and a bent capillary with a diameter d_0 and a curvature radius r_{curv} (b).

$$R_0(\theta) \simeq \left| \frac{2\theta}{(\varepsilon - 1)^{1/2}} - 1 \right|^2 \simeq 1 - 4\theta \,\mathrm{Im}\,(1-\varepsilon)^{-1/2}\,, \qquad \theta \ll 1\,. \tag{5}$$

Obviously, the coefficient of reflection of the beam as it turns through the large angle ϕ also depends on the number of reflections, N, which can easily be determined from the relation

$$N(\theta, \phi) = \frac{\phi}{2\theta}\,. \tag{6}$$

Thus, the total reflection coefficient is

$$R(\theta, \phi) = \big(R_0(\theta)\big)^N. \tag{7}$$

With allowance for the above relations, the coefficient of reflection of a grazing beam ($\theta \to 0$) as the beam is 'bent' by an angle ϕ is determined by the formula

$$R(0, \phi) = \exp\left[-2\phi \,\mathrm{Im}\,(1-\varepsilon)^{-1/2} \right]. \tag{8}$$

Analysis of this formula shows that when there is no absorption in the material of the reflecting surface ($\delta > 0$ and $\beta = 0$), the coefficient of reflection of the grazing beam is equal to unity, i.e., there is total external reflection as the beam propagates 'along' the curved surface. However, in real systems there is at least some absorption ($\beta \not\equiv 0$), so that $R(0, \phi)$ is smaller than unity. The imaginary part in (8) determines the coefficient of reflection of the grazing beam, and this coefficient is larger the smaller the absorption, i.e., the smaller the ratio β/δ. When $\beta/\delta \ll 1$, we have an expression for the coefficient of reflection of a grazing beam that has been turned through an angle ϕ in a form convenient for analysis [45, 46]:

$$R(0, \phi) \simeq \exp\left(-\phi\beta\delta^{-3/2} \right). \tag{9}$$

Note that, to the first approximation, this formula can be used for all angles smaller than the critical TER angle, since $\theta_c \ll 1$.

The above reasoning is also valid in the case where the reflecting surface constitutes a channel that is limited in space, i.e., an X-ray waveguide. A hollow glass capillary is an example of such a waveguide. Let us see how X-ray radiation is transported along such a capillary. Obviously, under certain conditions X-ray beams will propagate inside the capillary via multiple reflections from the capillary's walls (Fig. 1b).

Suppose that the source of X-ray radiation is located on the longitudinal axis of a straight ($r_{curv} \to \infty$) capillary at a distance l from its end. Of course, the optimal condition is $r/l = \theta_c$ (r is the inner radius of the capillary), since in this case all the rays emitted by the source at small angles $\theta \leqslant \theta_c$ will be captured by the capillary channel and transmitted over long distances, provided that the reflection from the surface is really good. Obviously, in this case the power of the radiation at the entrance of the capillary is given by the formula

$$W_1 = \frac{I_0 \theta_c^2}{4}\,, \tag{10}$$

where I_0 is the emission power of an isotropic source. The radiation power at the capillary exit is

$$W_2 = W_{21} + W_{22}\,, \tag{11}$$

where

$$W_{21} = \frac{I_0}{4}\left(\frac{r}{l+L}\right)^2 \equiv \frac{I_0 \theta_{min}^2}{4} \tag{12}$$

is the power of the radiation that passes through the capillary without reflection, with $\theta_{min} \equiv \theta_c(1 + L/l)^{-1}$ the smallest grazing angle for a beam of X-ray photons, and L the capillary's length. The power of the radiation that propagates via multiple reflections is determined by the second term on the right-hand side of Eqn (11):

$$W_{22} \simeq \frac{I_0}{2}\int_{\theta_{min}}^{\theta_c} R(\theta, \phi)\, \theta \, \mathrm{d}\theta\,. \tag{13}$$

Obviously, W_{21} can be ignored if the capillary is very long ($L/l \gg 1$). This situation is similar to the one in which the capillary is curved, so that there are no straight rays due to transillumination.

Now we can easily calculate the transmission coefficient (total reflection coefficient) of a single capillary:

$$k_{tr} = \frac{W_2}{W_1} \simeq \left(\frac{\theta_{min}}{\theta_c}\right)^2 + \frac{2}{\theta_c^2}\int_{\theta_{min}}^{\theta_c} R(\theta, \phi)\, \theta \, \mathrm{d}\theta\,. \tag{14}$$

The transmission coefficient, or transmissivity, actually characterizes the effectiveness of a capillary. The estimate of the above expression for an ideally reflecting surface ($R_0 = 1$) in the limit of $\theta_{min} = 0$ yields $k_{tr} = 1$, as expected.

The calculation of the term W_{22} is a problem in its own right. Assuming that the ratio of the distance from source to capillary exit to the channel radius is large ($(L + l)/r \gg 1$), we find that

$$W_{22} \propto L^{-1}\,\frac{L+l}{r} \gg \delta^{1/2}\beta^{-1}\,. \tag{15}$$

In other words, the radiation power inside the capillary decreases slower ($\propto L^{-1}$) than in free space ($\propto L^{-2}$). It is this fact that makes it possible to use capillaries for concentration and collimation of X-ray radiation. Moreover, substituting (15) in (14), we find that the greater the distance between source and target the higher the effectiveness of cylindrical waveguides.

When the capillary is curved, one must allow for the fact that not all rays entering the channel satisfy the condition $\theta \leqslant \theta_c$. If we assume that the inner radius r_0 of the capillary is small compared to the curvature radius r_{curv} of the bent capillary ($r_0/r_{curv} \ll 1$) and take into account the fact that the critical TER angle for X-ray photons is small ($\theta_c \ll 1$), the expression for the maximum value of the glancing angle can be written as follows [47]:

$$\theta_{max} \approx 2\left(\frac{r_0}{r_{curv}}\right)^{1/2}. \tag{16}$$

Hence, the conditions that must be met for the capture of radiation into the capillary transmission mode to be effective are

$$\theta_{max} \leqslant \theta_c\,, \quad \zeta \equiv \frac{r_{curv}\theta_c^2}{4r_0} \geqslant 1\,. \tag{17}$$

Obviously, the factor ζ determines the fraction of radiation captured by a curved capillary. For fixed curvature radii of the bend and the inner radius of the capillary, the smaller the energy of the incident photon the larger the value of this factor. At the same time, analysis of (17) shows that for the capillary to operate more effectively in the 'harder' region of the spectrum, the capillary radius must be decreased. Thus, the value $\zeta = 1$ determines the critical angle ϕ_1 through which a capillary of length L can be bent so that it operates effectively as an X-ray waveguide:

$$\phi_1 \equiv \frac{L}{r_{curv,1}} = \frac{L\theta_c^2}{4r_0}\,. \tag{18}$$

3.2 The effectiveness of capillary systems

Since the radiation power transmitted by a single capillary is very small because of the small aperture, it is advisable, in order to increase the aperture, to use a system of closely packed capillaries. When the packing is dense, the system consists of many capillaries arranged in layers around a central capillary. In the case of focusing capillary optics, each layer has its own curvature, which is the same for all capillaries in the layer. The curvature varies from zero for the central channel to a certain limiting value determined by the parameters of the system and source (see above) and the problem that has to be solved. There are three factors that determine the effectiveness of transmission for each layer: capture of radiation by the capillaries of the layer, absorption of radiation during transmission through the capillaries, and the number of capillaries in the layer. For layers close to the center of the system, the effectiveness of radiation transmission through a layer increases linearly with the number of channels, while for more distant layers in typical capillary systems the effectiveness drops due to the rapid decrease in the radiation capture by single capillaries and the increase in absorption. Hence, each layer effectively transmits gamma photons that belong to a certain energy interval, which in turn

requires optimization of capillary concentrating systems for specific problems.

Before we continue any further, let us clarify the terminology used in this review according to that adopted in the literature:

— a monocapillary is a single capillary;

— a polycapillary is a set of closely packed monocapillaries;

— a lens is a device that concentrates the radiation from a point source into a point (a small region);

— a half-lens is a device that concentrates a quasiparallel beam into a point or, in the reverse geometry, transforms the radiation from a point source into a quasiparallel beam;

— a monocapillary lens (half-lens) is a lens (half-lens) consisting of a bundle of identical monocapillaries closely packed in the transverse plane in such a way that the packing is strictly ordered;

— a polycapillary lens (half-lens) is a lens (half-lens) formed by polycapillaries. Present-day technology of polycapillary optics does not make it possible to align the channels of the different polycapillaries that form the polycapillary system, with the result that the polycapillary lens (half-lens) does not exhibit axial symmetry in its cross section.

Below we often use the terms capillary lens and capillary system in a generalized manner.

Let us estimate the effectiveness of a capillary system in controlling beams of X-ray radiation (note that our approach is valid not only for X-ray radiation but also for thermal and cold neutrons).

Since the critical TER angle for X-rays is small, the angular aperture of a monocapillary at its entrance is small, too (Fig. 2a):

$$\Delta\varphi_{\rm m} \propto \theta_{\rm c} \ll 1 \,. \tag{19}$$

This implies that the power transmitted by a monocapillary is small, too,

$$W_{\rm m} \propto \theta_{\rm c}^2 \; T_{\rm m} \,, \tag{20}$$

where $T_{\rm m}$ is the transmission coefficient, which depends on the geometrical parameters of the monocapillary and the quality of the inner reflecting surface of the channel. In the case of a monocapillary whose channel diameter diminishes from entrance to exit, a gain in radiation power of three or more orders of magnitude can be achieved at the monocapillary exit [48 – 50]. However, such systems are difficult to fabricate from the technical viewpoint, are very long, and are effective only in the case of quasiparallel sources of radiation of small transverse dimensions (in particular, third-generation sources of synchrotron radiation).

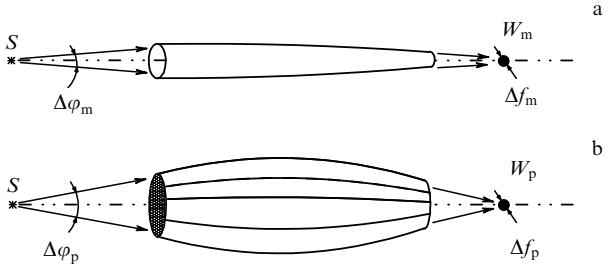

Figure 2. Focusing X-rays by (a) a monocapillary and (b) a system of capillaries (S is the source of X-rays, and Δf is the size of the focal spot).

The effectiveness of such systems can be increased by using polycapillary systems (Fig. 2b). Since the entrance angular aperture of a polycapillary system may be much larger than the critical TER angle,

$$\Delta\varphi_{\rm p} \gg \theta_{\rm c} \,, \tag{21}$$

the transmitted radiation power grows according to the formula

$$W_{\rm p} \propto (\Delta\varphi_{\rm p})^2 \; T_{\rm p} \gg W_{\rm m} \,, \tag{22}$$

where $T_{\rm p}$ is the transmission coefficient of the polycapillary system, assuming that the transmission through the system is not low ($T_{\rm p} \geqslant 10\%$). A polycapillary system designed in a certain way makes it possible not only to effectively transmit radiation but also to increase the radiation density $w \simeq W \,/\, (\Delta f)^2$ by focusing the radiation to a spot of size Δf. Hence, such a capillary system operates as a focusing lens.

Let us examine a capillary lens with an angular aperture $\Delta\varphi_{\rm p}$. If the transmissivity of the lens is $T_{\rm p}$, the power of the radiation focused to a spot of diameter $\Delta f_{\rm p}$ obeys the following expression:

$$w_{\rm p} \propto \pi \left(\frac{\Delta\varphi_{\rm p}}{2} \right)^2 \frac{T_{\rm p}}{(\Delta f_{\rm p})^2} \,. \tag{23}$$

Since the radiation density at a distance L from the source is inversely proportional to the distance, $w_0(L) \propto 1/(4\pi L^2)$, the use of a capillary lens makes it possible to achieve the following gain in radiation density:

$$G \equiv \left(\frac{w_{\rm p}}{w_0} \right)_L = \left(\frac{L\Delta\varphi_{\rm p}}{\Delta f_{\rm p}} \right)^2 T_{\rm p} \,. \tag{24}$$

The gain G determines the effective distance from the source of radiation at which radiation density without optics is equal to the radiation density at the focal spot of the capillary lens, i.e., $w_0(L_1) = w_{\rm p}(L)$. This yields the following convenient expression for calculating the effectiveness of the lens:

$$L_1 = \frac{L}{\sqrt{G}} = \frac{\Delta f_{\rm p}}{\Delta\varphi_{\rm p}\sqrt{T_{\rm p}}} \,. \tag{25}$$

Here, L_1 is the effective focusing length, which determines the distance by which the irradiated object is 'moved' closer to the radiation source. For instance, if the radiation density gain at the lens focus is 100, the effective proximity of the focus to the source decreases by a factor of 10. In addition, if we reduce the effective distance by a factor of approximately 3 by varying the parameters $\Delta\varphi_{\rm p}$, $\Delta f_{\rm p}$, and $T_{\rm p}$, the radiation density in the focal plane of the capillary system can be increased by a factor of 1000.

Present-day technology makes it possible to achieve effective proximity of the object to the radiation source amounting to only several millimeters, as estimates show. This considerably simplifies the organization of experiments since it solves one of the most pressing problems of the spatial arrangement of devices.

4. Wave theory of channeling

4.1 Propagation of waves in capillaries

We begin our discussion of the problems associated with the propagation of X-ray waves through capillary structures with the case of the interaction of electromagnetic waves with a surface in the limit of small glancing angles. The reflection of an electromagnetic wave is known to occur over an extended section of the surface and the minimum size of this section is determined in grazing reflection by $(\Delta d)_{\parallel\min} \sim (4\pi c/\omega_0)\,\theta_c^{-1}$, whose value is much larger than the distance between atoms. We can then assume that the scattering takes place in a macrofield characterized by a macroscopic dielectric constant $\varepsilon \simeq 1 - \theta_c^2$. This constant is the main characteristic of reflection and absorption of radiation in a layer of thickness $\Delta d_\perp \sim 2\pi c/\omega_0$ (e.g., for ordinary glass we have $\Delta d_\perp \approx 50$ Å). General analysis shows that, at glancing angles smaller than the Fresnel angle, total external reflection occurs. In the geometrical-optics approximation this means that scattering occurs primarily in the mirror direction and is coherent, while the incoherence is determined by the fraction of the radiation absorbed in the reflecting layer.

The propagation of X-ray radiation in capillary systems depends mainly on the interaction of the radiation with the inner walls of the channels. In the ideal case we can assume that the radiation beam is split into two beams, the reflected and the refracted. The latter proves to be strongly suppressed in total external reflection.

Usually a surface is characterized by its roughness, which determines the contribution of scattering to the reflection process. Here the scattered radiation propagates both inside the capillary walls and in the hollow part of the channel (a typical solid angle of dispersion is equal to 4π), thus forming a radiation distribution beyond the capillary. Hence, to determine the divergence of the radiation, one must solve the wave equation while taking account of the surface roughness. Mathematically this problem can be solved by introducing perturbations into the wave equation for an ideal surface [51], i.e.,

$$\left[\nabla^2 + k^2\varepsilon_0(\mathbf{r})\right]E(\mathbf{r}) = -k^2\Delta\varepsilon(\mathbf{r})E(\mathbf{r})\,, \tag{26}$$

where ε_0 is the dielectric constant of the medium, $\Delta\varepsilon$ is the perturbation of the dielectric constant related to the roughness of the surface, and $E(\mathbf{r})$ is the wave function of the radiation field, which can be written with allowance for roughness as follows:

$$E(\mathbf{r}) = \frac{1}{2\pi}\int u(r,\rho)\ \exp(\mathrm{j}\mathbf{q}\boldsymbol{\rho})\,\mathrm{d}^2\mathbf{q}\,, \tag{27}$$

with $\boldsymbol{\rho}$ the two-dimensional position vector in a plane parallel to the reflecting surface. Obviously, in the ideal case of a monochromatic wave ($k = \omega/c$), the integral in (27) can be simplified and represented in the form

$$E_i(\mathbf{r}) = u_i(r, q_i)\ \exp(\mathrm{j}\mathbf{q}\boldsymbol{\rho})\,, \tag{28}$$

where $q_i = k\cos\theta_i$, with θ_i the glancing angle of the incident wave.

The solution of Eqn (26) with boundary conditions imposed by the capillary channel shows that the radiation is redistributed between the coupled states, or modes, in the potential of the channel (see Section 4.2). What is important is that the channel potential operates as an effective mirror-reflecting barrier and, therefore, there is effective transfer of radiation by the hollow capillary tubes. Although the main fraction of the radiation undergoes incoherent diffuse scattering when it propagates in the capillaries, some of it propagates via coherent scattering, which is a special phenomenon, interesting both from the viewpoint of detecting such scattering in experiments and from the viewpoint of describing it [52, 53].

The scattering of electromagnetic radiation by a rough surface has been thoroughly studied and described within the scope of the general theory of diffuse scattering (e.g., see Refs [25, 54]). Using the general principles for the description of the process of propagation of X-ray radiation through a capillary ('channeling'), we can write the first-approximation expression for the relative intensity of scattering into the solid angle $\mathrm{d}\Omega$ as follows:

$$W_{is} \simeq \frac{\pi\omega^4}{c^4\theta_s}\left|D_{is}(\theta_s,\varphi_s)\right|^2\left|G_\mathrm{F}(\theta_s,\varphi_s)\right|^2\,, \tag{29}$$

where i and s are the quantum numbers corresponding to channeling modes, $D_{is}(\theta_s,\varphi_s)$ is the matrix element of the $i \to s$ transition, and $G_\mathrm{F}(\theta_s,\varphi_s)$ is the Fourier transform of the correlation function of the roughness of the reflecting surface. The total intensity W_i of the scattered radiation can be found by summing all the partial distributions W_{is}: $W_i = \sum_s W_{is}$. Estimates of these partial distributions become much easier if we examine their behavior in the meridional plane ($\varphi = 0$), which is an effective approach if we want to make simple and fast estimates of the radiation density behind the transport channels. Such simplification, however, may significantly change the angular distribution of the radiation (e.g., may have a strong effect on the estimate of the angular divergence of the radiation at the exit from a capillary or a system of capillaries).

4.2 A monocapillary as an ideal single waveguide

Let us now examine the propagation of X-ray photons inside a waveguide that is a hollow cylinder with an inner radius r_0. Since X-ray photons may be regarded as short-wave length electromagnetic waves, to establish the distribution of radiation in the monocapillary we solve the wave equation [55, 56].

The paths of X-ray photons in the channel with multiple reflection are spiral-like broken curves with different curvature radii, depending on the angle between the direction of the wave vector and the capillary axis. The radii of curvature of the particle paths vary from a minimum value equal to the radius r_0 of the waveguide channel to a maximum value determined by the curvature radius r_curv of the waveguide. Thus, assuming that the emission of X-ray photons is isotropic, in the first approximation we can postulate that the beam of photons is distributed continuously over all possible paths.

Let a particle travel along its path with a curvature radius r_1 that lies within the limits $r_0 < r_1 < r_\mathrm{curv}$. Thus, the problem reduces to the general problem of propagation of radiation $k = \omega/c = 2\pi/\lambda$ along a cylindrically curved surface with a curvature radius r_1:

$$(\Delta + k^2\varepsilon)\mathbf{E} = 0\,,\quad \varepsilon = \begin{cases} 1, & r < r_1,\\ \varepsilon_0, & r > r_1. \end{cases} \tag{30}$$

For the case of grazing-reflection optics it is obvious that while solving the wave equation we are most interested in the region near the interface, which actually determines the way in which the wave propagates during reflection. Using the well-known asymptotic methods [57–59], we arrive at the following formula for the radial distribution of radiation in the vicinity of $r \simeq r_1$:

$$\left|E_{\rm m}(\varrho)\right|^2 \propto \varrho\, K_{1/3}^2\left(\frac{2}{3}\,\varrho^{2/3}\right), \quad \varrho = r_1 - r \ll r_1\,, \tag{31}$$

where $K(\xi)$ is the modified Bessel (Hankel) function [60, 61]. The obtained solution of the wave equation in the region near the interface describes waves propagating along the walls of the waveguide. Here, the solution decreases as we move away from the channel walls toward the center; in other words, we have a solution for grazing modes that describes the structure of the electromagnetic field along a curved surface.

The above distribution can be used to estimate the characteristic radial size of the principal grazing mode ($m = 0$):

$$\overline{\varrho_0} \simeq 0.75\left(\frac{\lambda^2 r_1}{\pi^2}\right)^{1/3}. \tag{32}$$

Clearly, the characteristic radial size may be much larger than the wavelength of the wave propagating in the waveguide, since the curvature radius of the path of the photon in question may be much larger than the inner radius r_0 of the waveguide: $\overline{\varrho_0} \gg \lambda$. For instance, when $\lambda = 10$ Å, an estimate of $\overline{\varrho_0}$ made in the extreme case where $r_1 = r_0$ results in $\overline{\varrho_0} \gtrsim 75$ Å for a capillary with an inner radius $r_0 = 10$ μm.

Note that the distribution of the radiation flux behind the capillary is determined by the diffusely scattered radiation and by the radiation formed by various modes. Since usually only a few modes are 'populated' and their contribution to the total radiation flux is moderate, experimental observation of the structural changes in the angular distribution of the radiation behind the capillary is a difficult task. The situation may be improved by suppressing the diffusely scattered part of the radiation. This can be achieved by optimizing the parameters of the optical system in the experiment.

Calculations of the angular radiation distributions that allow for different channeling modes show that in capillaries of micron dimensions the beam divergence, determined by the modes with the smallest numbers, may be much smaller than the TER angle at a given energy (Fig. 3). However, if the number of modes is large, the divergence approaches the limit determined by the geometrical parameters of the capillary system.

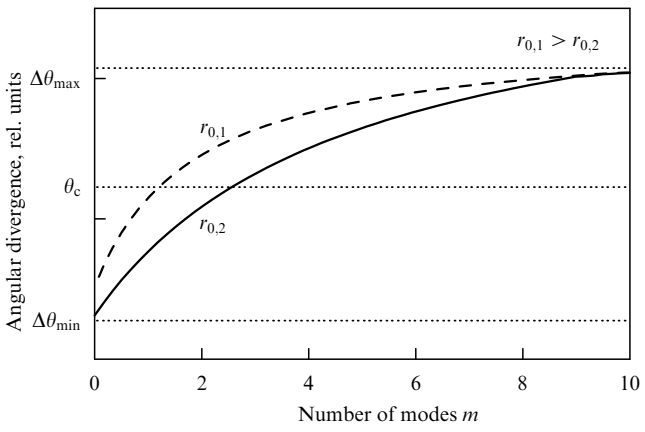

Figure 3. Divergence of a radiation beam behind a capillary system as a function of the number of modes m and the channel radius r_0.

4.3 Effect of surface roughness

Let us examine the scattering of radiation by a rough surface (Fig. 4). To simplify matters, we limit ourselves to a one-dimensional distribution, so that the equation of the surface is $z = z(x)$ instead of the real two-dimensional dependence $z = z(x, y)$. Then for an ideally smooth surface we have $z = 0$. With such a definition for the surface, the difference in the phases of randomly chosen incident ray and a ray scattered in the direction specified by the angle θ_s can be written as follows [25]:

$$\Delta\varphi \simeq kL(\theta_s^2 - \theta_i^2) + \Re\{z\}\,, \tag{33}$$

where L is the size of the reflecting surface, and $\Re\{z\}$ is the random roughness-distribution function over the surface $z = z(x)$. Since $z_{\max} \ll 2L$, we can assume that $\Re\{z\} \ll kL(\theta_s^2 - \theta_i^2)$. Hence, $\Delta\varphi \gg 2\pi$ or, in other words, the scattering of radiation by a rough surface in the nonmirror direction is always incoherent. However, in the case of mirror reflection $\theta_s = \theta_i$, the phase of the wave can be estimated by the formula

$$\varphi \simeq 2k\left(1 - \frac{\theta_i^2}{2}\right)z(x), \quad \theta_i \to 0\,, \tag{34}$$

which suggests that φ is constant for a smooth surface or that the field is coherent.

Generally speaking, it must be noted that in reality there are no pure (coherent or incoherent) states. The average scattered power $W_s \propto \langle E_s E_s^* \rangle$ is determined by all scattering processes and can be written in the form of the sum $\langle E\rangle\langle E\rangle^* + \delta\{E\}$, where the first term is responsible for coherent scattering and the second for incoherent scattering. When the surface is ideally smooth, i.e., $\delta\{E\} = 0$, which means that $\langle EE^*\rangle = \langle E\rangle\langle E\rangle^*$, we have coherent waves. In the other extreme case, when the surface is very rough, we have $\langle E\rangle\langle E\rangle^* = 0$, which means that $\langle EE^*\rangle = \delta\{E\}$, and only incoherent waves are reflected from the surface. Between these two extreme cases, which are the pure states of the reflected field, there is real redistribution, i.e., usually we are dealing with a continuous transition from coherence to incoherence (see also Ref. [62]).

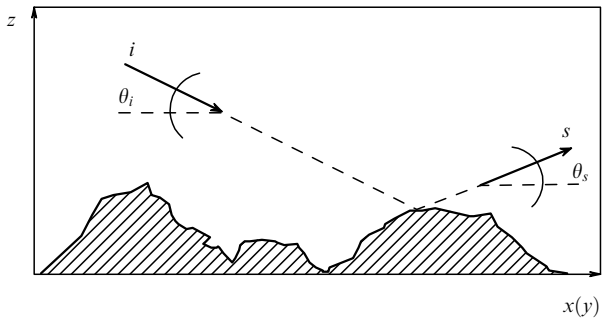

Figure 4. Schematic representation of the scattering of radiation by a rough surface during reflection.The angles θ_i and θ_s will be called here the incidence and scattering angles, respectively.

Let us now discuss the case of periodically distributed roughness and again limit ourselves to one-dimensional geometry (only the longitudinal direction of the capillary is taken into account), i.e., $z(x)$ is a periodic function with a period a of the profile of the inner surface of the capillary wall: $z(x) = z(x + a)$. Such a pattern may arise because of the mechanical drawing of the heated capillary. Analysis of the general relationships for radiation scattering easily produces the following dependence between the angles of incidence and reflection (scattering):

$$\theta_{s,l} = \theta_i + l\,\frac{\lambda}{a}\,. \tag{35}$$

This formula shows that the dispersion scattering diagram is formed by narrow-directed peaks observed at certain angles (35),

$$W_{s,l} = \frac{1}{I_{s,l}}\,\frac{\mathrm{d}I_l}{\mathrm{d}\Omega} \propto \left|R(\theta_i)\sqrt{\varepsilon(\theta_i)}\,\right| |\alpha_l|^2 \left|R(\theta_l)\sqrt{\varepsilon(\theta_l)}\,\right|, \tag{36}$$

where α_l is the weight factor of scattering in the direction $\theta_{s,l}$, and $|\varepsilon(x)| \simeq x^2 \pm 2l\lambda/a - (l\lambda/a)^2$. Since in the X-ray range the condition $l\lambda/a \ll 1$ is held, dispersion is at its maximum at small grazing angles $\theta_i \to 0$; as a result, we obtain

$$W_s \propto \theta_i\sqrt{\varepsilon(\theta_i)}\,\sum_l |\alpha_l|^2\,\theta_l\sqrt{\varepsilon(\theta_l)}\,. \tag{37}$$

Obviously, this formula may be more complicated and contain characteristic peaks. The principal peak manifests itself in the direction of mirror reflection (coherent scattering), while the broadening in the angular distribution of radiation emerges because of incoherent scattering. Note that within the range of angles and roughness parameters in question, the dispersion of radiation occurs mainly at angles larger than the incidence angle (Fig. 5). However, the coherent part of the radiation, determined by the factor that stands in front of the sum in (37), $\langle E(\theta_s)\rangle\langle E(\theta_s)\rangle^* \neq 0$ practically for all scattering angles. Furthermore, at small values of the period a, the angular distribution of the scattered radiation has a tendency to increase the scattering at large angles. In the scattering spectrum there appears an additional maximum at angles that exceed the angle of incidence onto the inner surface of the capillary. This fact suggests that the coherent component of scattering acquires a nonmirror peak because of the wavy periodicity of the interaction potential: $\partial'_\theta\left(\langle E(\theta)\rangle\langle E(\theta)\rangle^*\right)|_{\theta=\theta_1>\theta_c} = 0$; however, this has no noticeable effect on the power of the radiation transmitted by the capillary.

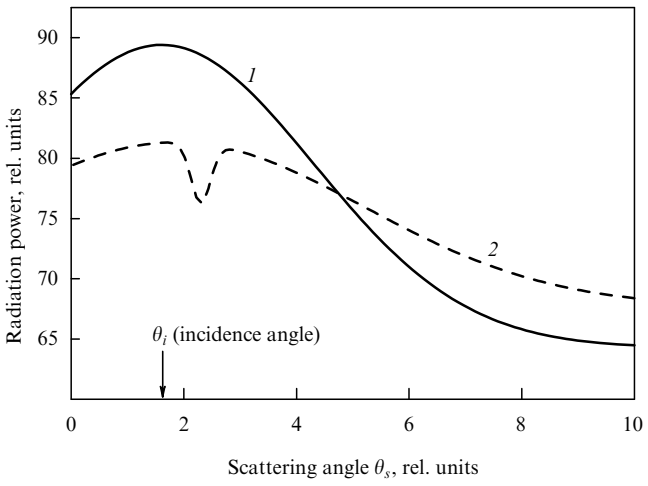

Figure 5. Angular scattering in a capillary with a periodically distributed roughness of the surface for two different relations between the roughness period a and the transverse wavelength $\lambda_\perp$: *1*, $a \gg \lambda_\perp$ and *2*, $a \sim \lambda_\perp$. The angle of incidence on the wall is marked by a vertical arrow. \

The main remarks made in connection with this special case are also valid for a surface-roughness periodicity of an arbitrary nature.

Even in the earlier works (for more details see Ref. [15]) the scattering of radiation by surfaces with randomly distributed roughness was studied in detail. There, it was shown that in the limit of small grazing angles the main characteristics of scattering are described by the formula

$$W_s(\theta_s) \propto (k\theta_i)^3\,R(\theta_i)\,\varkappa(\theta_s,\theta_i)\,\zeta(\theta_{si})\,, \tag{38}$$

where $k\theta_i \simeq (k_\perp)_i$ is the transverse vector of the incident wave,

$$\varkappa(\theta_s,\theta_i) \simeq \left(\frac{\theta_s}{\theta_i}\right)^2 \frac{\left|\theta_i + \sqrt{\varepsilon - 1}\,\right|^2}{\left|\theta_s + \sqrt{\varepsilon - 1}\,\right|^2}\,,$$

and $\zeta(\theta_{si})$ is the roughness function, with $\theta_{si} \equiv (k_\perp)_i\,|\theta_s - \theta_i|$. Here correlation analysis of Eqn (38) in relation to the beam and surface parameters was carried out on the assumption that the scattering is at its maximum in the mirror direction, i.e., $\theta_{si} = 0$. The results of such analysis have shown that in the case of single scattering from a rough surface the observed peak manifests itself either in the mirror direction or in a direction between the angles θ_c and θ_i.

However, such an approximation cannot be used in multiple-reflection optics and, in particular, in capillary optics. As noted earlier, at grazing angles in systems with multiple reflection there is what is known as surface channeling of photons [63–65], which substantially modifies the nature of the radiation distribution in the channels. Owing to the presence of coupled states on the surface, the angular distribution has a peak at angles $\theta_{s,\max} \lesssim \theta_i$. By solving the wave equation (26) with the boundary conditions for a capillary waveguide, we can estimate the angular distribution of the radiation scattered in a capillary. Calculations of the intensity of the radiation scattered by a capillary wall with a mean-root-square roughness height ξ and a correlation length σ [which means with a correlation function $G(x) = \xi^2\exp(-x/\sigma)$], done according to the formula

$$W_s(\theta_s) \propto \frac{\xi^2\sigma}{\theta_s\left[1 + (\sigma\Delta k)^2\right]^{3/2}}\,\sum_l \left|E_l(\theta_s)\right|^2, \tag{39}$$

where $E_l(\theta_s)$ is the angular function of a photon in the coupled state l, lead to the result shown in Fig. 6. The diagrams show that the angular distributions of the scattered radiation change dramatically with correlation length: the effect of roughness becomes noticeable at correlation lengths comparable to the transverse wavelength of the scattered photon, $\sigma \sim \lambda_\perp \gg \lambda$ ($\gamma \equiv \sigma/\lambda_\perp \gtrsim 1$). Note that at certain values of the roughness parameter, some of the radiation is scattered to angles smaller than the incidence angle. Moreover, theoretical calculations have shown that such scattering can also be observed in the case of a smooth surface of a certain curvature (scattering in a capillary is scattering by a

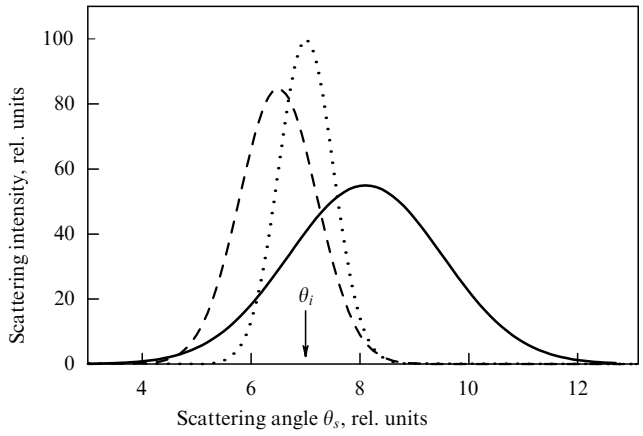

Figure 6. Scattering of radiation with initial divergence $\Delta\theta_i$ in a capillary for different values of the roughness parameter γ: · · ·, incident beam, $\Delta\theta_i$; – – –, $\gamma = 100$, $\Delta\theta_s/\Delta\theta_i = 1.4$; ——, $\gamma = 1-10$, $\Delta\theta_s/\Delta\theta_i = 2.9$.

curved surface). This fact can be explained by the capture of some portion of radiation into coupled (bound) states, i.e., by surface channeling. The remaining part of the radiation travels through the capillary channels and is diffusely scattered [65–67].

When $\gamma \lesssim 1$, the average transmitted radiation power is determined chiefly by the incoherent component, i.e., $\langle EE^* \rangle \simeq \delta\{E\}$, but the coherent component still exists, although it becomes very small ($\langle E \rangle \langle E \rangle^* \to 0$). When $\gamma \gg 1$, the contribution of the coherent component increases and the scattering becomes partly coherent and partly incoherent, at the same time. Note that in this limit there may be small-angle diffraction of the reflected rays, a phenomenon predicted by Compton (see [68]). In this case some of the features observed in the angular distribution can be explained by the presence of coherent scattering in the process of interaction of radiation with the reflecting surface.

The above suggests that the roughness of the inner reflecting surface of the capillary may significantly change the angular radiation distribution after the radiation is transmitted through the capillary, with the transmitted radiation power not changing significantly.

4.4 A system of capillaries: a polycapillaries

When we turn to a system of X-ray waveguides (capillaries), we find that the solution of the general wave equation becomes very complicated and is impossible in analytic form. Hence, the solution of the problem of how the periodicity of capillary systems affects the way in which X-ray waves propagate through such structures requires the use of numerical methods [64, 69].

As is known, the motion of a photon in a medium whose characteristics are determined by the dielectric constant $\varepsilon(\omega, \mathbf{r})$ (here $(\mathbf{r} \equiv (\mathbf{r}_\perp, z) \equiv (x, y, z)$ is the position vector of the photon) is described by the wave equation (30) [51]. In our case the medium through which the photon travels is a system of hollow waveguides (capillaries). Let us assume that in the cross section, i.e., in the (xy) plane, the given system is rigorously ordered and possesses hexagonal symmetry. Here, it is obvious that the coefficient of reflection of an X-ray wave from the walls of the channel (for the sake of convenience, we introduce a new designation n), being a function of the photon energy, position vector, and the angle of incidence on the walls of the channels, is a spatially periodic function. Thus, we have a situation similar to the one observed in the channeling of charged particles in crystals. Hence, to solve the wave equation we can use the well-known numerical method of solution for equations of motion in periodic fields [70, 71].

Under boundary conditions at the entrance to the capillary system in the form $E(\mathbf{r})|_{z=0} \equiv E(\mathbf{r}_\perp, 0)$, the transport problem for the photon beam is solved at each step Δz by the well-known splitting procedure [72, 74]

$$E(\mathbf{r}_\perp, z_i + \Delta z) = (\hat{F}\hat{I}\hat{F})\, E(\mathbf{r}_\perp, z_i)\,. \tag{40}$$

The splitting procedure makes it possible to separately examine the free propagation of the wave

$$\hat{F} \equiv \exp\left(-\frac{\mathrm{i}\Delta z}{2}\,\frac{\nabla_\perp^2}{(\nabla_\perp^2 + \omega^2)^{1/2} + \omega}\right) \tag{41}$$

and the change in phase as the wave is reflected from the walls

$$\hat{I} \equiv \exp\left[-\mathrm{i}\Delta z\, \xi(\omega, \mathbf{r})\right]. \tag{42}$$

The function $\xi(\omega, \mathbf{r})$ in formula (42) for the operator $\hat{I}$ describes what is known as the interaction potential between the photon and the channel walls and may be written as follows:

$$\xi(\omega, \mathbf{r}) = \omega\big(n(\omega, \mathbf{r}) - 1\big)\,. \tag{43}$$

At each step Δz, the propagating wave is expanded in a two-dimensional Fourier series [74] with a limited number N of terms, which is determined by the computational grid imposed on the unit cell:

$$E(\mathbf{r}) = \sum_{m=-N/2+1}^{N/2} \sum_{n=-N/2+1}^{N/2} E_{mn}(z) \exp\left[\mathrm{i}\omega(\mathbf{e}_\omega \mathbf{r}_\perp)\right], \tag{44}$$

where $|\mathbf{e}_\omega| = 1$. The latter allows an exact numerical representation of the propagation equation to be obtained. The value of N in expansion (44) depends on the length L of the computational grid,

$$\frac{N\pi}{L} > \omega \sin\beta\,, \tag{45}$$

and the maximum value of the angle β between the direction of propagation of the plane wave with the transverse wave vector (ω_x, ω_y) and the z axis:

$$\sin\beta = \frac{(\omega_x^2 + \omega_y^2)^{1/2}}{\omega}\,. \tag{46}$$

Calculations according to this procedure can be done for two different cases. In one case the X-ray waves propagate through a system of hollow capillaries arranged in such a way that in the cross section there is exact hexagonal symmetry. What is more, the system captures the quasiparallel beam and focuses it at a certain focal distance. The results of calculations of the flux intensity for X-ray waves in the focal spot are shown in Fig. 7a. Clearly, the focal spot exhibits a structure with distinct symmetry: there is a strong central maximum against the background of symmetrically arranged subsidiary maxima. What is interesting is that the characteristic widths of the observed maxima are close to the channel dimensions at the lens exit and that the redistribution of the intensity in the

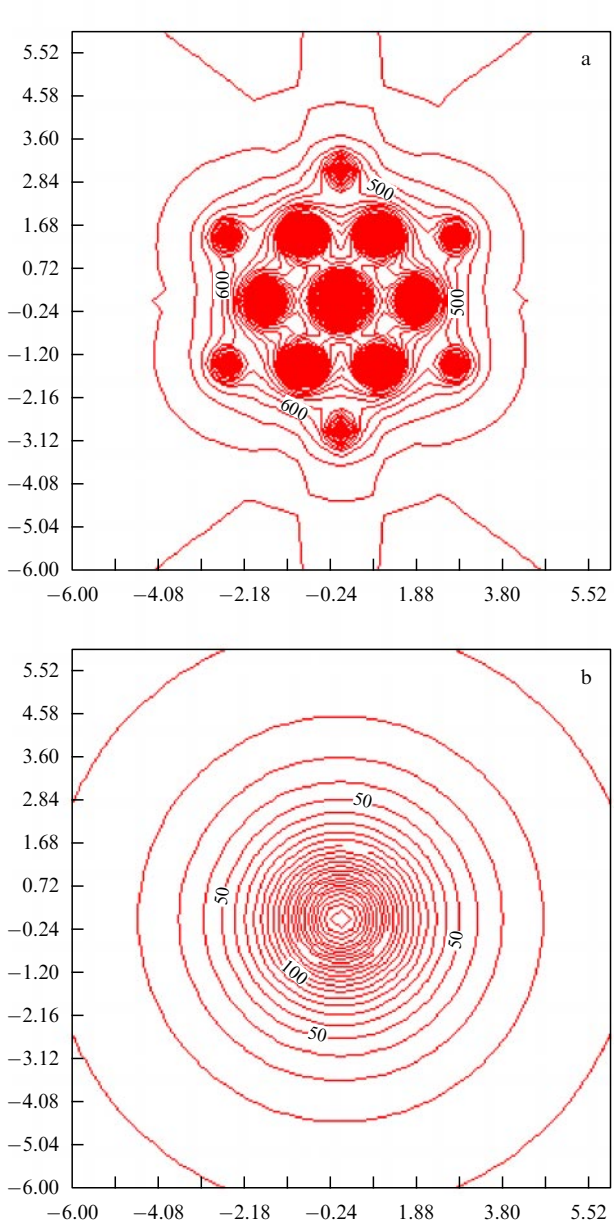

Figure 7. Structure of the focal spot of a lens with (a) ordered and (b) disordered arrangement of capillaries in the cross section of the capillary system.

focal spot leads to the formation of a strong central peak (a first-order maximum).

In the other case the waveguide capillaries in the lens are arranged chaotically in the transverse plane of the system. The interference pattern observed in the ordered lens disappears (Fig. 7b); instead, there is a broad single maximum in the focal spot. The width of the focal spot for such a lens coincides with the ordinary classical estimate of the size of a focal spot [75] and is much larger than the capillary diameter at the lens exit.

The observed interference structure of the focal spot of focused radiation can be explained by the phase buildup caused by a spread in the length of paths traveled by photons in different capillary layers. One must bear in mind, however, that this is not enough for the interference properties to manifest themselves in the focal spot. Analysis has shown that the packing of the capillaries in the cross section of the lens must exhibit a definite symmetry (quadratic, orthorhombic, hexagonal, etc.). The interference effect is not observed if the capillaries are packed at randomly.

The interference pattern is also observed for lenses consisting of planar structures, e.g., systems of planes bent in a certain way. This effect is observed with X-rays, thermal neutrons, electromagnetic radiation in the visible part of the spectrum, and charged particles, provided that certain stringent conditions are met. Furthermore, the effect is observed with straight capillary columns when the radiation falls on one of the ends of such columns. Here, of course, the channels of each column must be packed in a certain symmetric way.

5. Some analogies in capillary systems

5.1 Geometrical (ray) analysis of the wave approximation

Research in the focusing of synchrotron radiation by capillary structures has shown that the spot of X-rays focused by a half-lens has a certain structure [52, 53, 76]. The fact that the focal spot has a structure cannot be explained in terms of ordinary geometrical (ray) optics. According to ray-optics calculations, the focal spot is a structureless bright spot of X-ray radiation. The characteristic size of the spot can be estimated by the following formula [75]:

$$\Delta f \approx d_2 + 2\theta_c f, \tag{47}$$

where d_2 is the inner diameter of the channels at the lens exit, θ_c is the critical TER angle, and f is the focal distance of the lens in question at its exit. Obviously, for capillaries of micron diameters d_2 we have $d_2 \ll 2\theta_c f$, with the result that the size of the focal spot is much larger than the capillary diameter. Values provided by (47) are in good agreement with experimental data. However, it is impossible to study the structure of the focal spot in this approximation.

The passage of photon beams through capillary systems is in a certain sense similar to the channeling of fast charged particles in crystals [77 – 79].

The reader will recall that when a charged particle flies into a crystal, it may be captured into the channeling mode, provided that the angles of its direction of motion with respect to the principal crystallographic axes or planes are small. In other words, the channeling of charged particles requires that the angles at which the particles enter the crystal in relation to the crystallographic axes or planes be smaller than a certain critical channeling angle $\psi_1 \simeq (2U_0/\omega)^{1/2}$ (ψ_1 is known as the Lindhard angle), where U_0 is the depth of the potential well representing the interaction of an impinging particle and the crystal (a characteristic of the crystal), and ω is the particle energy.

In dealing with the channeling of photons in hollow capillary structures we also have to deal with a very strong angular dependence. Indeed, the coefficient of reflection of X-rays from various materials increases as the angles of glancing in relation to the channel walls decrease, and approaches unity at angles smaller than the critical TER angle θ_c. Note that θ_c depends on the photon energy and on the type of material from which the optical system is made. The analogy becomes even more perfect if we allow for the fact that in some capillary lenses there is a certain packing order: there is symmetry both in the transverse plane and in the longitudinal.

Thus, a capillary lens is in a certain sense a macrocrystal. However, many parameters of the capillary structure may be controlled (in contrast to crystals), which is very important in solving a number of application problems.

Let us examine a system that focuses a quasiparallel beam of X-ray photons. We assume that the system consists of many capillaries that are closely packed in such a way that there is a hexagonal symmetry in the cross section of the system. Obviously, in this case the capillary diameters decrease from the maximum value d_1 at the lens entrance to the minimum value d_2 at the exit. Thus, the capillaries are packed into layers, with each layer i having its own curvature radius $r_{\mathrm{curv},i}$. Since the capillaries are bent (except for the central one), it is obvious that in some cases not all photons that fly into the system will be channeled. Hence, on the entrance end of the lens we can isolate 'active' areas (the photons that land in these areas will be channeled) and 'inactive' areas (in such areas the angle of incidence of photons on the channel walls are larger than the critical angles, with the result that such photons are mostly absorbed). Figure 8 depicts a typical pattern of the filling of capillaries at the lens entrance, which in the first approximation can be replaced by a more simple axisymmetric pattern. Clearly, at the lens entrance we have a system of concentric rings with widths defined by the formula [75, 80]

$$\delta_i \simeq \frac{r_{\mathrm{curv},i}\,\theta_c^2}{2}\,. \tag{48}$$

Then the corresponding radius of the inner (r_i) and outer (r_i') circles that limit the rings are

$$\begin{aligned} r_i &= \left(i+\frac{1}{2}\right)d_1 - \delta_i\,,\\ r_i' &= \left(i+\frac{1}{2}\right)d_1\,. \end{aligned} \tag{49}$$

Bearing in mind that $|1 - r_{\mathrm{curv},1}/r_{\mathrm{curv},2}| \ll 1$ and $|\varphi_1 - \varphi_2| = \Delta\varphi \ll 1$, which means that $|r_{\mathrm{curv},1}\varphi_1 - r_{\mathrm{curv},2}\varphi_2| \simeq r_{\mathrm{curv},1}\Delta\varphi$, we arrive at the following formula for the difference of the paths of closely located rays (by no means necessarily from different layers: $\Delta L \approx \Delta r_{\mathrm{curv}}\,\varphi\theta_c^2/2$. It is obvious that, by varying the angle φ and the negligibly small difference in the curvature radii $\Delta r_{\mathrm{curv}} \equiv |r_{\mathrm{curv},1} - r_{\mathrm{curv},2}|$, we can satisfy the well-known condition of interference $\Delta L = m\lambda/2$, where λ is the radiation wavelength and m is the order of the interference maximum. For example, if the energy of the quantum is $\omega \simeq 30$ keV ($\theta_c \simeq 1$ mrad), $\varphi \simeq 0.1$ mrad, and $\Delta r_{\mathrm{curv}} = 0.1-1$ cm, we obtain an estimate $\Delta L = 1-10$ Å for the difference in the ray paths. Note that we consider a more general problem (with several parameters) as compared to the conventional interference optical elements.

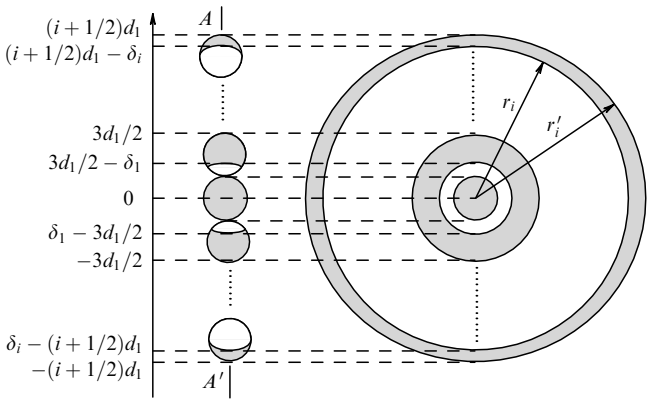

Figure 8. Diagram of the filling of capillaries at the entrance end of a capillary system. In the first approximation the real pattern of 'active' areas can be replaced by a system of concentric rings. It is assumed that the central channel is completely filled, or $r_{\mathrm{curv}}\theta_c^2 = d_0$.

Following the above argumentation, we can easily obtain an expression for the areas of the 'working' rings. Since, in the case of capillary lenses, the relation $\delta_i \propto \Delta r_i$ is valid, we can estimate the area of the ith ring using the formula $S_i \simeq 2\pi r_i\,\delta_i$. Therefore, taking into account that $r \propto i$ and using expression (48), we obtain $S_i \propto i r_{\mathrm{curv},i}$. It is known that the curvature radius $r_{\mathrm{curv},i}$ decreases with increasing layer number i; therefore, if we take $r_{\mathrm{curv},i} \propto 1/i$, then the ring area will be independent of the position on the butt end of the lens. From the equality of the ring areas, we obtain an expression that relates the radii of curvature of neighboring zones and the widths of the zones with the diameter of the lens channels at the entrance,

$$1 - \frac{r_{\mathrm{curv},i+1}}{r_{\mathrm{curv},i}} = \frac{1}{\zeta_i + i + 1/2}\,, \tag{50}$$

where $\zeta_i = \delta_i/d_1$ is the parameter determining the extent to which a particular channel is filled.

The above analysis shows that at the exit of a lens with ordered packing we have a pattern similar to that of zone plates, which suggests that it is possible to observe the wave properties of X-ray photons focused by capillary lenses. But how can interference effects manifest themselves in channels that are so large (compared to the wavelengths of the radiation propagating in these channels)?

Below we will see that when X-ray photons travel through capillary systems, in view of the extreme smallness of the grazing angles there is a kind of surface channeling of X-ray waves inside the channels: part of the beam is captured into a coupled state (a subbarrier state) determined by the channel parameters, while the rest of the beam propagates in the quasi-free mode (above-the-barrier state). It is the presence of coupled motion that explains the coherence in the superposition of waves transported by hollow channels. One must bear in mind, however, that not all of the radiation flux is redistributed in the process of scattering through the capillaries. Both the coherently scattered waves from the subbarrier states and the incoherently scattered waves (diffuse scattering) contribute to the formation of the structure of the spot beyond the capillary system. It must be noted that the diffusely scattered waves are usually predominant in the general flow of waves propagating in capillary channels, so that it is difficult to detect the effect in experiments.

5.2 Quantum description of grazing reflection

Recently it has been shown [52] that the propagation of X-ray photons in a capillary system is a highly complex phenomenon. Not all the features observed in experiments can be explained in terms of geometrical (ray) optics [81–83]. The use of methods of wave optics, on the contrary makes possible a detailed description of the processes of propagation of radiation in capillaries.

The transmission of X-rays through capillary systems is generally determined by radiation interaction with the inner walls of the channels. In the ideal case, where the inner walls

are ideally smooth surfaces, the beam is split into two beams, the mirror-reflected and the refracted. The latter proves to be highly suppressed in the event of total external reflection of the radiation from the channel wall. The characteristics of scattering of the radiation by a capillary channel can be estimated from the solution of the wave equation. In the first approximation, in which the surface roughness is ignored, or $\Delta\varepsilon(\mathbf{r}) = 0$ ($\Delta\varepsilon$ is the perturbation of the dielectric constant caused by the roughness of the reflecting surface), the wave equation in the direction perpendicular to that of the radiation propagation can be written as

$$\left[\nabla_\perp^2 - k^2\delta(r_\perp) + k_\perp^2\right]E(r_\perp) = 0\,, \tag{51}$$

where E is the radial wave function of the radiation and $\mathbf{k} \equiv (k_\parallel, k_\perp)$ is the wave vector.

Since at grazing angles ($\theta \ll 1$) the transverse component of the wave vector is $k_\perp \approx k\theta$, the 'effective potential' of the interaction between the radiation beam and the surface can be written as follows [84]:

$$V(\mathbf{r}_\perp) \simeq k^2\left[\delta(r_\perp) - \theta^2\right] = \begin{cases} -k^2\theta^2\,, & r_\perp < r_1\,, \\ k^2(\delta_0 - \theta^2)\,, & r_\perp \geqslant r_1\,, \end{cases} \tag{52}$$

where r_1 corresponds to the position of the reflecting surface. This, incidentally, leads to the quantum mechanical definition of total external reflection, where the effective potential is zero ($V = 0$), and to the formula for the Fresnel angle (the angle at which TER is observed), $\theta \equiv \theta_c \simeq \sqrt{\delta_0}$.

If the reflecting surface is curved, the effective interaction potential acquires an additional term, which corresponds to additional 'potential energy.' The physical meaning of this energy amounts to the following. Due to the curvature of the reflecting surface, which is specified by an angle φ, in the interaction with the surface the photon acquires an angular momentum $kr_{\mathrm{curv}}|_\varphi$, where r_{curv} is the curvature radius of the 'selected path' of the photon, and φ is the azimuthal angle in cylindrical coordinates along the direction of propagation of the radiation (in the case of a capillary in the form of a hollow cylindrical tube, the direction of propagation may not coincide with the longitudinal axis z of the capillary, or $(\widehat{\mathbf{k}, \mathbf{e}_z}) \neq 0$). As a result, the expression for the effective potential acquires the term $-2k^2 r_\perp / r_{\mathrm{curv}}$:

$$V(r_\perp) \simeq k^2\left[\delta(r_\perp) - \theta^2 - 2\,\frac{r_\perp}{r_{\mathrm{curv}}}\right]. \tag{53}$$

Clearly, the expression for the interaction potential in the case of a planar surface, (52), follows from the general expression (53) for a curved surfaces with $r_{\mathrm{curv}} \to \infty$. The change in the potential is shown schematically in Fig. 9. As the spatial parameters of the system change, the interaction potential transforms from steplike with a barrier of height $k^2\delta_0$ for the planar surface to a potential well whose width and depth are determined by the channel characteristics. Note that an increase in curvature (or a decrease in the curvature radius) leads to an increase in the well's depth and hence to an increase in the number of coupled states. When the potential gradient is small, the wave features of the radiation in the process of scattering from the surface become negligible, and the problem of radiation propagation can be solved by the methods of geometrical (ray) optics.

Below we will briefly discuss the solution of the wave equation in the case of an ideally reflecting surface (no roughness), when the reflected beam is formed mainly by the coherently scattered part of the radiation (see Refs [56, 63]). The solution of the wave equation with the boundary conditions for a capillary channel shows that X-ray radiation may be distributed over coupled quantum states, which are determined by the potential of the capillary channel. What is important is that the channel potential is an effective reflecting barrier, with the result that there is effective transmission of X-ray radiation through hollow capillary tubes. With a real surface, the main part of the transmitted radiation undergoes incoherent diffuse scattering [85], while the remaining part (usually a very small part) is determined by coherent scattering [86].

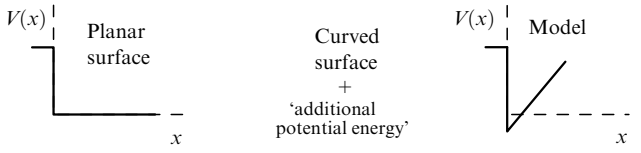

Figure 9. Schematic representation of the change in the radiation interaction potential caused by reflection from a planar surface and a curved surface. The presence of curvature leads to the appearance of a potential well.

Let us estimate the extreme value of the curvature radius of the reflecting surface, $r_{\mathrm{curv,\,max}}$ (in the case of a capillary the value of the curvature radius depends on the parameters of the capillary or the system of capillaries and the way in which the capillary is bent and also on the plane in which the propagation of radiation is examined), at which the wave properties of the radiation propagating along the surface may manifest themselves [87]. We take a photon (i.e., we specify the wave vector $\mathbf{k}$) interacting with a surface whose curvature radius is $r_{\mathrm{curv},\,i}$ (i determines the selected path along which the radiation propagates). At small grazing angles θ the variation of the longitudinal (i.e., along the direction of propagation) wave vector $k_{||}$ is negligible; it is mainly the transverse component of the wave vector, $k_\perp$, that changes:

$$k_\perp \simeq k\theta \quad (\theta < \theta_c)\,. \tag{54}$$

As this formula implies, the transverse component of the wave (the transverse wavelength) is much larger than the radiation's wavelength, which makes it possible to observe interference effects even for very short wavelengths. Indeed,

$$\lambda_\perp = \frac{\lambda}{\theta} \gg \lambda\,. \tag{55}$$

As is known, to observe the wave properties in the process of photon scattering the typical size of the 'effective channel' δ_i in which the radiation actually propagates must be comparable to the photon's effective wavelength (in our case, the transverse wavelength, since at very small grazing angles $\theta \ll 1$ we cannot ignore the change in wavelength as we go over to transverse coordinates), i.e., $\delta_i(\theta) \simeq \lambda_\perp(\theta)$ (Fig. 10). For a capillary this quantity coincides with (48). Bearing in mind that δ_i depends on the curvature radius $r_{\mathrm{curv},\,i}$ of the surface for a selected direction i and an angle θ of incidence of radiation on the surface, we can write the following criterion for the coupled propagation of radiation along the curved surface in the form

$$r_{\mathrm{curv},\,i}\,\theta^3 \sim \lambda\,. \tag{56}$$

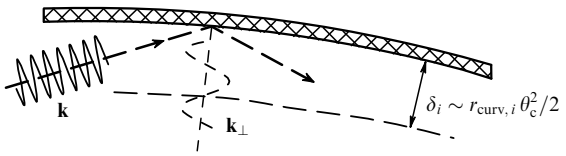

Figure 10. Schematic representation of the propagation of radiation with a wave vector **k** along a curved surface with an effective transverse channel size $\delta_i \simeq r_{\mathrm{curv},i}\theta_c^2/2$.

This relationship yields $r_{\mathrm{curv,max}} \sim 10$ cm for a photon with a wavelength $\lambda \sim 1$ Å at a grazing angle $\theta \simeq \theta_c/3$. Thus, simple analysis produces a useful formula that describes surface-coupled propagation of radiation, i.e., surface channeling of X-ray photons along a curved surface and, in particular, in the microchannels of capillary systems (see also Ref. [88]). Moreover, formula (56) suggests that the wave properties of X-ray photons may manifest themselves in microcapillary systems.

6. The transition from microchanneling to nanochanneling

Capillary optical elements consist of hollow drawn tubes through which radiation is transmitted via multiple reflection from the inner walls of the channels [49, 50]. However, microcapillary systems are also of interest as wave-optics elements, i.e., drawn and bent capillaries are capable of operating as X-ray waveguides [89]: capillary optics may be interpreted as 'whispering-gallery optics.' It is a well-known fact that the physical meaning of whispering-gallery optics amounts to multiple reflection of radiation formed by a large number of bunches [46]. The total angular aperture of such a device is determined by the number N of bunches and the grazing angle θ of the beam and is equal to $2N\theta$. Since the reflection of a single bunch from a surface with a complex-valued dielectric function ε is determined by the coefficient

$$R_{1\{{}^{s}_{p}\}} \simeq 1 - 2\theta\,\mathrm{Re}\left[\left\{{1 \atop \varepsilon}\right\}(\varepsilon - 1)^{-1/2}\right], \tag{57}$$

where s and p are polarization indices of the radiation, the total reflection can be estimated in the limit $\theta \to 0$ ($N \to \infty$) as follows:

$$R_{\{{}^{s}_{p}\}} \simeq \exp\left[-\left(1 - R_{1\{{}^{s}_{p}\}}\right)N\right]. \tag{58}$$

Estimates made according to these formulas show that whispering galleries are capable of effectively transporting radiation in a selected narrow frequency range [90].

The use of wave theory to explain the transmission of radiation through capillary structures makes it possible to describe the fine effect of redistribution of radiation in the channels of these systems [64, 69, 87]. Below we will see that the process of transporting radiation by capillary optical systems is extremely complicated. Radiation can be divided, by convention, into two parts: one part propagates by scattering that obeys geometrical (ray) optics, while the other part is captured into coupled states by the surface potential of the reflecting surface and is described by the wave equation of propagation. As the channels become smaller and their diameter approaches the transverse wavelength of the radiation, surface channeling is replaced by bulk channeling similar to the channeling of charged particles in crystals [77, 91–94]. Today, the technology of manufacturing capillary systems makes it possible to fabricate samples with channel sizes in the submicron range [95]. If the channels are made even smaller, we move into the nanometer range, and then carbon nanotubes (there is considerable progress in fabricating such nanotubes [96]) replace microcapillaries as new optical nanosystems (provided that we know how to control the orientation of nanotubes in space) [97, 98].

A carbon nanotube [99–101] may be thought of as a small capillary (on the nanometer scale). Its wall consists of carbon atoms ordered in space, with the distance between the atoms being approximately 1–2 Å. The typical diameter of a single nanotube is estimated at approximately several dozen angstroms (the ratio of channel diameter to wall thickness can reach two orders of magnitude), while the length of such a tube may reach submicron values. All this suggests that we must use the wave approximation if we want to solve the problem of transmitting radiation through nanotubes. In this case a carbon nanotube can be considered as an X-ray waveguide, a fact vividly demonstrated by a channeling theory developed for the purpose of describing the process of propagation of radiation through such structures [102, 103].

Calculations involving various aspects of channeling and the study of the channeling of beams of charged particles in carbon nanotubes suggest that it is possible to observe the channeling effect in experiments involving both straight and bent nanotubes [104–107].

6.1 Surface channeling in microcapillaries

In the case of capillaries, the waveguide is a hollow cylindrical tube, so that, if we ignore the absorption of radiation in the course of reflection from the inner walls of the capillaries, the interaction potential, which determines the way in which the radiation propagates, can be written in the form of (53), where $\delta_0 \simeq \theta_c^2$ is the polarization parameter. The wave equation can be represented in terms of normalized (dimensionless) cylindrical coordinates $\mathbf{r} \equiv (r_\perp, \varphi, z)$. Since what interests us most about the problem of propagation of radiation through capillary structures is the region near the inner surface of the walls, we select a system of coordinates with its z axis directed along the direction of propagation of radiation. Thus, the solution of the wave equation characterizes the grazing propagation of waves near the surface of the reflecting wall, $r_\perp \simeq r_1$; in other words, it determines the wave packet of radiation along a path with a curvature radius r_1.

Hence, by representing the transverse coordinate in the form $r_\perp = r_1 - \rho$, $|\rho| \ll r_1$, we can write the wave equation for the coordinate ρ with a fixed curvature of the path. Here, the curvature radius can be varied from the minimum value r_0, which corresponds to the capillary radius, to the maximum value r_{curv}, determined by the curvature of the capillary, i.e., $r_0 \leqslant r_1 \leqslant r_{\mathrm{curv}}$. Such a transformation of the coordinates makes it possible to substantially simplify the mathematical problem and reduce it to solving the radial wave equation. Dropping the details of calculations, we simply write the general solution of the equation:

$$E_n \simeq \sum_m C_m u_m(\rho)\exp\left[\mathrm{i}\,(k_\parallel z + n\varphi)\right],$$
$$u_m(\rho) \propto \begin{cases} \mathrm{Ai}\,(\rho + \rho_m), & \rho > 0, \\ \alpha\mathrm{Ai}'(\rho_m)\,\exp(\alpha\rho), & \rho < 0 \quad (\alpha > 0), \end{cases} \tag{59}$$

where the prime stands for the derivative with respect to ξ, $\mathrm{Ai}(\xi)$ is the Airy function, which is the solution of the differential equation $\mathrm{Ai}''(\xi) = \xi\,\mathrm{Ai}(\xi)$ (it falls exponentially for $\xi > 0$), ρ_m is the mth zero of the Airy function, and $\alpha = \delta_0^{-1/2}(2/kr_1)^{1/3}$ [64]. Obviously, these expressions are valid only for modes with small indices and near the surface of the channel walls; in other words, (59) determines the structure of the grazing modes of radiation inside the transmission channel (Fig. 11).

This solution also shows that the wave functions exponentially decay as we move deeper into the reflection wall, $\rho < 0$ [like $\exp(-2|\alpha||\rho|)$], and as we move away from the wall toward the channel's center, $\rho > 0$ (a property of the Airy function). Note that the mode nature of the radiation propagation in the hollow part of the capillary occurs without any distortions of the wavefront. Analysis of the above relations also suggests that almost all the power of the radiation is accumulated in the hollow part, with the result that there is only weak suppression of radiation along the walls of the waveguide.

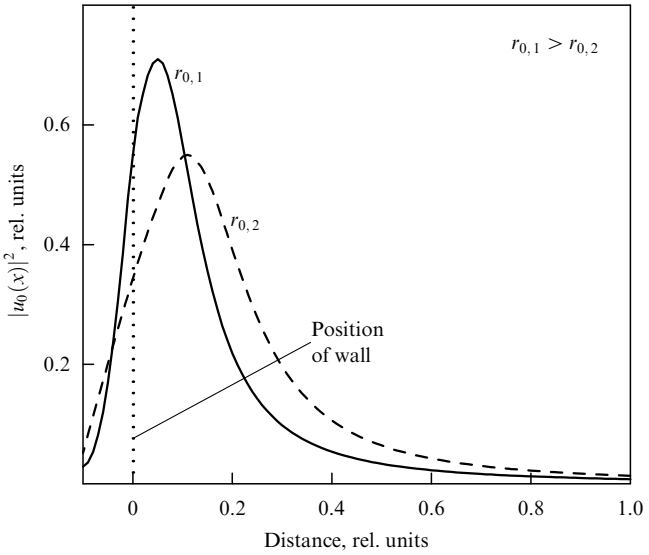

Figure 11. Radial distribution of radiation in the channel of a capillary system for two different capillary radii. The vertical dotted line indicates the position of the wall.

6.2 Bulk channeling in nanocapillaries

Above we examined the transmission of X-ray beams through capillary systems with channel dimensions in the micron and submicron ranges. Obviously, in this case we are dealing with surface channeling (the propagation of radiation along the channel walls), since the channel dimensions exceed the wavelength by nearly three orders of magnitude. The effect of bound transmission of radiation can be observed because the reflecting surface is curved. However, the situation changes substantially when the dimensions of the channels become comparable to the wavelength of the radiation (the nanometer scale). In practice, this means that the diffraction angle for the selected wave, which is defined as $\theta_\mathrm{d} = \lambda/d$, with d the capillary diameter, becomes comparable to the critical TER angle. In other words, the photon's transverse wavelength approaches the diameter of the transmission channel: $\lambda_\perp/d \sim 1$. Here, instead of surface channeling we have bulk channeling and, in the first approximation, with a small potential gradient caused by curvature we can ignore the contribution of the longitudinal curvature. Thus, photon channeling (which is not surface channeling in this case) in the channels of capillary systems is possible even when there is no curvature, i.e., we can speak of a real X-ray guide, just as in fiber optics. Moreover, under certain conditions, when the channels in the cross sections of the system are arranged in a certain order, capillary nanosystems become like crystals, which in turn makes it possible to use the well-known tools of the theory of particle channeling in crystals with small entrance angles with respect to the principal crystallographic directions [102, 103].

Typical nanotubes consist of carbon atoms which, as they become organized into crystalline hexagons, or fullerenes, form the walls of a cylindrical surface with the graphite structure, so that if we 'unroll' the cylinder we get a graphite film (Fig. 12; in this figure the fullerene molecule is represented by the image of a small soccer ball). Here the nanotube wall may be either single-layer or multilayer. In this way an axisymmetric channel is formed, and the channel is a potential well that determines the way in which radiation is transmitted by the nanotube. The effective interaction potential is determined by the plasmon energy, which varies from the center of channel to wall and can be estimated by the formula

$$\omega_\mathrm{p}(r) = \left(\frac{4\pi N_0(r)\,e^2}{m_0}\right)^{1/2}, \qquad (60)$$

where e and m_0 are the electron charge and mass, and $N_0(r)$ is the density of the electron cloud in the nanotube at a distance r from the center of the channel (it is at its minimum at the center of the channel and at its maximum at the wall). Depending on the model chosen for the calculation of the atomic potential $f(\mathbf{k})$ (the Molière potential, the Doyle–Turner potential, etc.), and hence on the averaged atomic potential of the chain $V_R(\rho)$ and on the averaged atomic potential for the nanotube $U(\mathbf{r})$, we can write different expressions for the electron density $N_0(\mathbf{r})$ (see Fig. 12), but all this only affects the accuracy with which the radiation

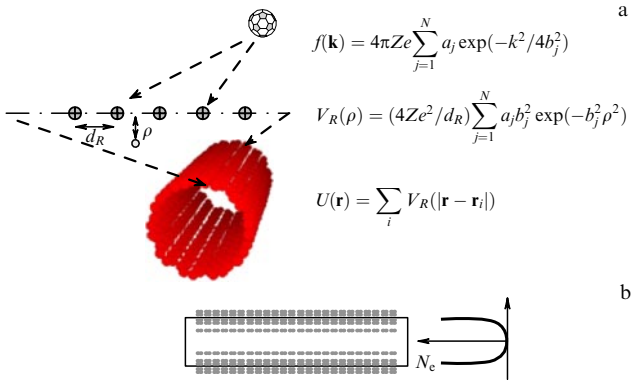

Figure 12. Schematic representation of the formation of a cylindrical channel of a nanotube: (a) carbon compounds known as fullerenes (the 'soccer ball') form chains which, in turn, form the walls of the nanotube. The right-hand side of the figure shows the expressions for the interaction potentials, where for the chain and nanotube the potentials are averaged over all elements that form the chain and nanotube, respectively; (b) the electron distribution N_e in the nanotube channel with its maximum near the wall and its minimum at the channel's center.

scattering process is described, leaving the main features unchanged. The radiation propagates in a medium with a variable dielectric constant

$$\varepsilon(r,\omega) = 1 - \frac{\omega_p^2(r)}{\omega^2}\,, \tag{61}$$

which also depends on the radiation frequency ω; this implies that photons with higher energies experience total external reflection from the nanotube wall at smaller distances from the wall. Since the higher the density of the electron cloud (which happens as we move closer to the nanotube wall) the larger the absorption of radiation, there is filtration of the beam according to energy as the radiation is transmitted by the nanotube. What is more, nanotubes of radius r_{curv} bent at a certain curvature radius r_0 are also capable of deflecting the beams, provided that

$$\frac{4r_0}{r_{curv}} \leqslant \frac{\omega_p^2(r)}{\omega^2}\,. \tag{62}$$

Let us now mathematically analyze the way in which radiation is transmitted by systems consisting of oriented nanotubes. Today, the most advanced technology is that of fabricating nanotubes with multilayer walls, and so we discuss precisely such a system. We begin by simplifying the problem of transmission of radiation by a real nanosystem: we examine only the radial wave equation. This will enable us to ignore the presence of curvature in the interaction potential, which is important if we want to prove that there can be bulk channeling without curvature. Thus, our system is a multilayer planar waveguide with a central channel of diameter d_0 and a period d between the adjacent layers forming the system. For such a waveguide the interaction potential can be written in the form

$$V(r) = \sum_n V_n(r) = k_r^2\left[-1 + \Delta\sum_n \delta\left(|r| - \frac{d_0}{2} - nd\right)\right], \tag{63}$$

where $\Delta \equiv \bar{\delta}_0 d$ is the spatially averaged polarizability of the material of the reflecting wall, $k_r^2 = k^2 - k_z^2$, and $\delta(x)$ is the Dirac delta function with the independent variable x. Taking into account the boundary conditions and the symmetry of the potential, we find that for the central channel with $|r| \leqslant d_0/2$ the solution of the equation of propagation in the transverse plane is given by the simple expression

$$E_0(r) = \begin{cases} a\cos k_r r\,, & \text{even mode,} \\ a\sin k_r r\,, & \text{odd mode.} \end{cases} \tag{64}$$

Now we can find the solution of the wave equation for the first layer $d_0/2 \leqslant |r| \leqslant d_0/2 + d$ in the form of a linear combination of waves propagating in opposite directions: $E(r) = b\exp(ik_r r) + c\exp(-ik_r r)$. Since the potential (63) is a periodic function, $V(r) = V(r+d)$, this solution must obey the Bloch theorem $E(r+d) = \exp(i\varkappa d)E(r)$, where $\varkappa$ is a complex quasi-momentum: $\varkappa \equiv \operatorname{Re}\varkappa + i\operatorname{Im}\varkappa$. Bearing in mind this fact and solving the wave equation for the given boundary conditions, we arrive at the following expression for the parameter $\varkappa$:

$$\exp(2i\varkappa d) - 2\left[\cos k_r d - \frac{k^2\Delta}{k_r}\sin k_r d\right]\exp(i\varkappa d) + 1 = 0\,. \tag{65}$$

Accordingly, joining the solutions of the wave function and its derivative in the plane $|r| = d_0/2$, we obtain the dispersion relations for the even and odd modes of the channeled wave:

$$\begin{aligned} \tan\frac{k_r d_0}{2} &= -\frac{k^2\Delta}{k_r} + \frac{\cos k_r d - \exp(i\varkappa d)}{\sin k_r d}\,, \\ \cot\frac{k_r d_0}{2} &= \frac{k^2\Delta}{k_r} - \frac{\cos k_r d - \exp(i\varkappa d)}{\sin k_r d}\,. \end{aligned} \tag{66}$$

The latter are reduced to the solution of the standard eigenvalue problem of the transport of radiation by a multilayer system with a period d both in the presence of a central gap ($d_0 \gg d$) and in a spatially isotropic medium ($d_0 = d$). Obviously, we are interested in the specific case of a narrow channel with $d_0 = d$, which corresponds to a multilayer nanotube. The wave functions of the allowed modes in this case are described by the formula

$$E_n(r) \propto \begin{cases} \cos k_r r\exp(ik_z z)\,, & -\dfrac{d_0}{2} \leqslant |r| \leqslant \dfrac{d_0}{2}\,, \\ \propto \cos\dfrac{k_r d_0}{2}\,\dfrac{\exp(i\varkappa r)\sin(k_r|\tilde{r}|) - \sin\left(k_r(|\tilde{r}| - d)\right)}{\sin k_r d} & \\ \times\exp\left[i(\varkappa nd + k_z z)\right]\,, & \dfrac{d_0}{2} + nd \leqslant |r| \leqslant \dfrac{d_0}{2} + (n+1)d\,, \end{cases} \tag{67}$$

where $|\tilde{r}| \equiv |r| - d_0/2 - nd$. We see that equations (66) have only even solutions with a definite quasi-momentum

$$\exp(i\varkappa d) \simeq 1 - \frac{k^2(d - d_0)}{2}\Delta\,. \tag{68}$$

The imaginary part in the expression for the quasi-momentum,

$$\operatorname{Im}\varkappa = \frac{k^2}{2}\left(1 - \frac{d_0}{d}\right)\operatorname{Re}\Delta$$

determines the dependence of the mode amplitude on the distance from the channel's axis. What is important is that the even mode exists at all ratios of the channel size to the size of the reflecting layer and is characterized by a decrease of order

$$\frac{k^3}{4}\left(1 - \frac{d_0}{d}\right)^2 \operatorname{Re}\Delta\operatorname{Im}\Delta$$

in the longitudinal attenuation factor $k_z = \sqrt{k^2 - k_r^2}$. The spatial distribution has a maximum at the center of the channel and local singularities caused by tunneling through the potential barrier of the layers. Figure 13 shows the radial wave function in a system with a well-defined central channel and a multilayer wall with a period that is twice as small as the channel size. Analysis of this distribution shows that there is exponential attenuation of the wave as the distance from the nanotube axis grows, $\exp(-|\operatorname{Im}\varkappa|r)$, with a certain structure manifesting itself near the walls of the multilayer nanotube because of the presence of local maxima of the wave functions at the nanotube walls. The general formula (68) shows that for an isotropic system (with well-defined channels, e.g., crystals) we have $\operatorname{Im}\varkappa = 0$, which is an indication that there is no localized mode.

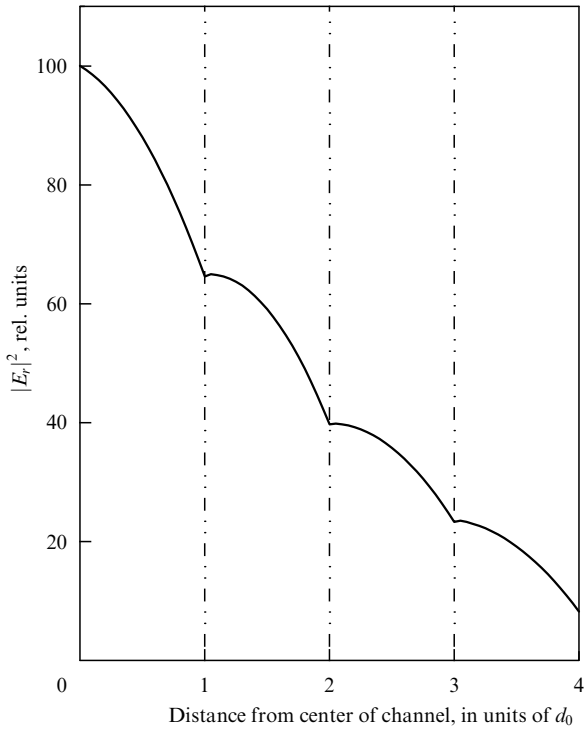

Figure 13. Radial distribution of radiation in a multilayer nanostructure in which the size of the central channel is twice the distance between the layers forming the nanowall.

The width of the main mode can be found from the relationship $|\operatorname{Im}\varkappa|^{-1} \approx 100-1000$ Å and may be much larger than the diameter of the nanotube channel ($\lesssim 100$ Å even in the case of a multilayer nanotube). As noted earlier, since the nanotube walls are so thin, part of the radiation in the process of channeling in the central channel tunnels through the potential barrier of the wall. A simple analysis of the propagation of radiation in such systems shows that the main channeling mode (the main bound mode) is present in any such structure, while higher modes may be suppressed at certain dimensions of the channels. Hence the interest in nanotubes as wave guides with controllable modes. Moreover, it would be interesting to study the scattering of radiation in nanosystems with multilayer walls. In this case there could be diffraction of the waves reflected from different layers of the wall, and this may have a marked effect on the radiation distribution behind the nanosystem.

Miniaturization of capillary structures and the discovery of a new class of natural nanosystems, carbon nanotubes, has placed the problem of studying the transmission of X-ray photons by such systems on an entirely new level. Analysis shows that when the channel diameter is in the micron range, surface channeling of photons begins to play an important role in the mechanism of radiation transmission (part of the radiation is redistributed in the channel when it is captured by the curved surface into a coupled mode). Such a transmission mechanism substantially changes the angular distribution of the radiation after transmission through the capillary system. As the channel dimensions become smaller and reach the nanometer scale, the mechanism of coupled transmission of radiation in such systems changes, with surface channeling replaced by bulk channeling. Thus, the entire radiation in nanostructures undergoes mode transmission, in contrast to the transmission of radiation by microstructures, where only a fraction of the radiation is coupled by the interaction potential.

As we have seen above, thin carbon nanostructures may serve as a basis for developing new devices that use the mode nature of transmission of X-ray radiation through such structures, as ordinary waveguides do at optical frequencies [108]. Of course, the effectiveness of nanomaterials in solving applied problems must still be studied, irrespective of the importance of the problem we are discussing here from the standpoint of fundamental physics.

7. Features of radiation redistribution by capillary systems

As the popularity of capillary optical elements grew, researchers found that it was possible to use this new optics to focus synchrotron radiation [109–113]. The fact that capillary lenses can increase the density of synchrotron radiation was first demonstrated on the C-60 FIAN synchrotron [110] (for the parameters of the source of synchrotron radiation see Refs [114, 115]). The results of these experiments were found to be in good agreement with the theoretical estimates done in the framework of geometrical (ray) optics.

Theoretical calculation based on the wave approach have shown that structural changes manifest themselves in the focal spot of a symmetric monocapillary half-lens (see Section 4.4) [87]. In a series of independent experiments that followed these calculations (see Refs [116, 117]) it was found that there is strong redistribution of radiation behind capillary lenses, and the first interference patterns proving such redistribution were obtained.

The first experiment used a monocapillary half-lens. This lens was fabricated, according to a special technology, of glass monocapillaries in such a way that in the transverse plane the capillaries formed a close hexagonal packing and their diameters varied continuously from entrance to exit. The diameters of the several hundred capillaries that formed the lens were 1.0 and 0.6 mm at the entrance and exit, respectively; the length of the lens and the focal distance were 45.5 and 40.0 mm, respectively; and the open area at the entrance amounted to about 70%.

The X-ray radiation was filtered in energy, with the result that a narrow band was cut from the broad energy spectrum, which was then sent through the lens. All the elements of the system were placed inside a vacuum chamber maintained at a pressure of about 5×10^{-6} Torr, which ensured strong suppression of scattering and absorption of the initial beam. The chamber made it possible to record the radiation at different distances from the half-lens exit (from 0 to 175 mm). The vertical angular width of the beam of synchrotron radiation at half-maximum amounted to 1 mrad for a wavelength of 10 Å. All experiments were carried out at a distance of 7 m from the emitting point on the electron orbit. The angular precision of the alignment of the half-lens axis along the X-ray beam was no less than 2.5 mrad. In the experiments the photon beam was focused from an area of 30 mm in diameter at the half-lens entrance to a focal spot with a diameter less than 3 mm.

The experiment consisted of several series. The first series was carried out with a monochromatic beam of X-rays with a photon energy of about 1 keV (a wavelength of 12.4 Å) propagating in the monocapillary system. Figure 14 is the digitized X-ray image of the radiation that passed through the

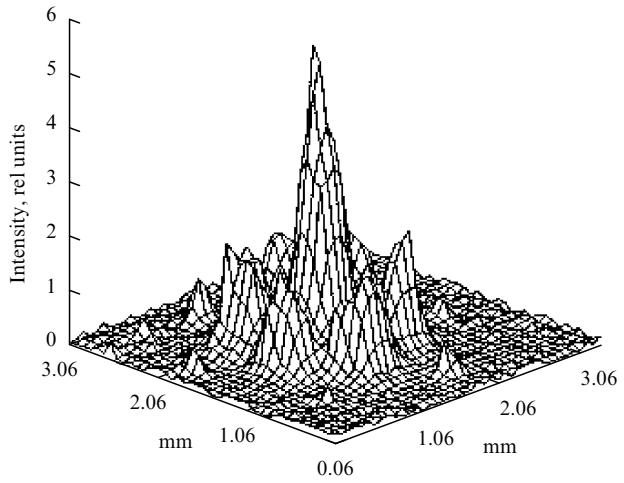

Figure 14. Distribution of radiation at the focus of a monocapillary structure. A characteristic feature of the monostructure is the presence of order in the cross section of the channels.

half-lens (in the focal plane). We see that the focal spot has a very definite structure consisting of interference peaks. The diameter of the entire focal spot, defined according to formula (47), amounts to 3 mm, which agrees with the experimental data. However, the width of the central peak, as the experimental data and the results of calculations show, is about 0.6 mm, which amounts to one-fifth of the spot diameter estimated within the framework of geometrical (ray) optics.

The picture changes dramatically when a polycapillary system replaces the monocapillary lens. The distribution of the transmitted radiation at the focus is shown in Fig. 15. Clearly, all the features of the previous result have disappeared; instead of a structured focal spot, we have a broad maximum whose geometrical dimensions are in good agreement with those that follow from geometrical (ray) optics.

To verify the correctness of the results, a new series of experiments with monocapillary systems irradiated by a beam of X-ray photons ($\sim$ 1.5 keV) was conducted. These experiments studied the changes in the observed pattern obtained by closing different parts of the ends of the half-lens. The results of measurements for an open end, a closed central part, and a closed sector supported the assumption that the interference in the focal spot is the result of diffraction of X-rays in the capillary half-lens; despite the mask that blocked the passage of radiation (closed sector), the interference structure overlapped the classical shadow of the mask. Interesting results were also obtained in the scanning of a beam of focused radiation with a wavelength $\lambda = 13.3$ Å beyond the focus. Here the incident beam did not fill the entire entrance end of the half-lens; on the diametrically opposite sides there remained areas not filled with radiation in the form of half-moons with the greatest thickness equal to a quarter of the end's radius. On the exit end two central capillary layers were closed. It was found that in this case the interference pattern changes dramatically; instead of a structure with interference peaks, there was one with a whole set of bright straight lines (similar to Kikuchi lines in X-ray photographs of crystals) against the background of the diffuse spot. These lines intersect and thus represent the symmetry of the capillary-structure channels.

A similar pattern was also observed in the case of a conical monocapillary system. Figure 16 shows the X-ray image of the focal spot recording the beam of synchrotron radiation with an energy of about 1.5 keV. As in other cases with a symmetrical arrangement of the channels, the image clearly exhibits a structure with its maximum at the center of the spot and symmetrically (hexagonally) arranged side maxima against the background of a blurred diffuse pattern.

In the propagation of X-ray photons in capillaries we are dealing with small-angle multiple reflection. In this connection it would behoove us to examine the interaction between the transverse wave of electromagnetic radiation and the channel walls, assuming that the longitudinal wave remains almost the same. Here the length of the transverse wave is much larger than the radiation wavelength. At the same time, due to the smallness of the grazing angles, the photons, while propagating in the channel, will mainly fill only a narrow region near the wall, i.e., the effective channel within which the photons move has a very small transverse dimension, much smaller than the channel diameter. Thus, the real dimensions of channels (corridors) of propagation and the interaction wavelengths become comparable, which makes

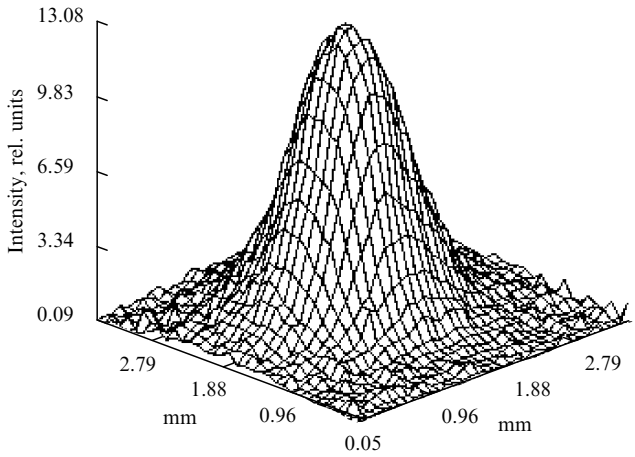

Figure 15. Distribution of radiation at the focus of a polycapillary structure. The structure has no order in the cross section of the channels.

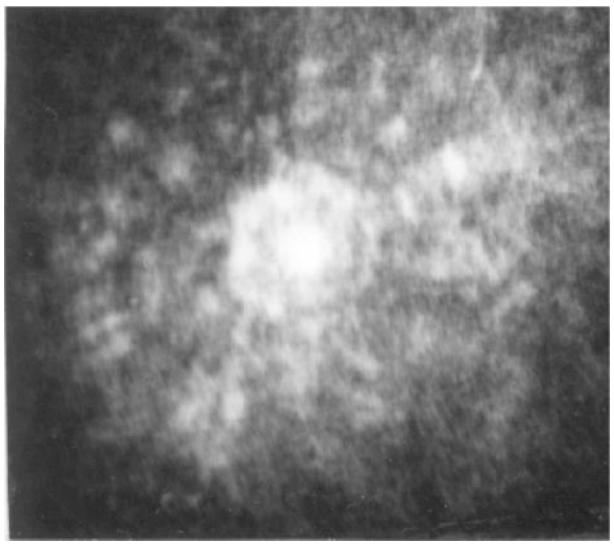

Figure 16. X-ray image of the focal spot of a conical monocapillary system.

possible the manifestation of the wave properties of X-rays as this radiation is transmitted by periodic capillary structures. Of course, part of radiation propagates not along the channel walls but fills a large transverse area of the channels: this part obeys the laws of geometrical (ray) optics and does not participate in the creation of the interference pattern.

Theoretical calculations have shown that the conditions that must be met so that interference in the focus of capillary focusing systems can be observed are extremely stringent. The first condition requires strict periodicity in the cross section of the capillary system. Violation of this condition destroys the interference of X-ray waves transmitted by the system. This fact has been proved in the experiment in focusing synchrotron radiation by a polycapillary half-lens. Note that a polycapillary system differs from a monocapillary system in that inside every 'macrochannel' it contains many 'microchannels' whose symmetry of arrangement is not the same as in the neighboring macrochannels.

Another necessary condition is that the capillary systems must focus the radiation at the same focal distance. If different layers of the capillary packing have different focuses, there can be no interference. This fact has been thoroughly studied using specially manufactured half-lenses [118].

The organization of the experiment is also subject to strict requirements, since obtaining reliable results requires exact alignment of the focusing system along the beam. The importance of this aspect is suggested by the dependence of the intensity of the focused radiation on the angle between the beam of synchrotron radiation and the half-lens axis, obtained for different divergences of the incident beam. Calculations have shown that a misalignment equal to the critical TER angle θ_c leads to a decrease in the intensity in the focal spot for a parallel beam ($\Delta\theta = 0$) by 5% and for beams with divergences $\Delta\theta = \theta_c$ and $\Delta\theta = 2\theta_c$, by 40 and 50%, respectively. Here we must take into account the fact that even with ideal alignment to the beam the intensity decreases by 10 and 50% for divergences equal to the critical angle and twice the critical angle, respectively. But if the misalignment with respect to the beam amounts to only $2\theta_c$, the intensity of radiation in the focal spot drops to almost zero in all cases. The results of the experiment in transmitting a beam of X-ray radiation through capillary half-lenses support the theoretical data: under variations of the angle between beam and system amounting to 2.5 mrad, the transmissivity changed by almost 15%.

The C-60 synchrotron channel was used to carry out a series of experiments in focusing soft X-rays by separate capillaries [55, 56, 82]. An interesting result was obtained when the radiation was focused by two capillaries bent in a special way. These capillaries reunited beams of radiation that had passed through them in a single plane. The parameters of the system were determined by optimizing the problem in order to meet the necessary physical conditions and from the technological standpoint (when the system is not too miniature). The installation and alignment of the system ensured at the entrance the smallest possible angles between the direction of propagation of the radiation and the tangents to the longitudinal axes of the capillaries. The system included a diaphragm at the entrance to the capillary system that was used to 'irradiate' the capillaries either one after another or simultaneously. In both cases the focusing occurred at the same point, allowing a comparison of the characteristics of the distribution of the radiation intensity behind the system of

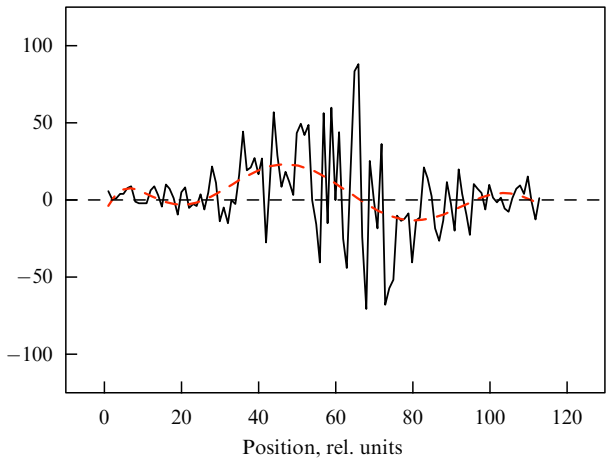

Figure 17. The interference curve for the case of an optical system consisting of two bent microcapillaries. \

two capillaries. The detection system made it possible to digitize the images and therefore build an experimental curve describing the difference in the radiation distributions for the cases described above (Fig. 17). As expected, the result corresponds to the interference term in the integral of the focused radiation when both capillaries are irradiated simultaneously. In other words, there is an explicit redistribution of radiation caused by the superposition of waves. The possibility of observing the wave properties of X-rays after transmission through capillary or similar systems has also been discussed in later works of different researchers [81, 119 – 121].

According to a recent report [65], under certain conditions one can observe a decrease in the angular divergence of an X-ray beam after transmission through a capillary system. A significant difference was discovered between the values of the angular divergence of FWHM observed in the experiment and those predicted by the geometrical (ray) theory of radiation propagation in capillaries (Fig. 18). For instance, the expected divergence of a beam of synchrotron radiation was estimated to be of order $2\theta_c \simeq 0.9^\circ$ at an energy of 4 keV. This value exceeds both the experimentally observed value ($\mathrm{FWHM}_{exp}[4\ \mathrm{keV}] = 0.28^\circ$) and the value after a Gauss fitting

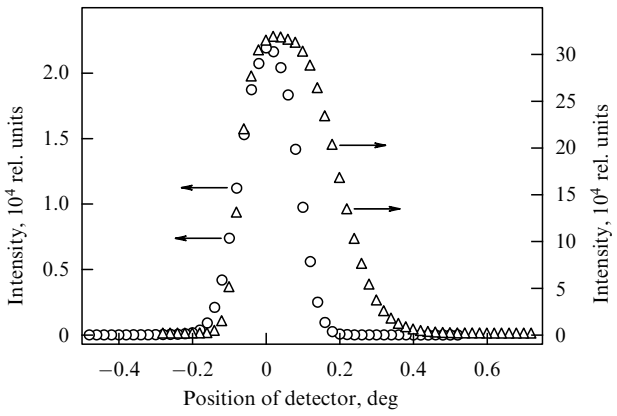

Figure 18. The experimentally measured angular divergence of radiation after propagation through a capillary system: ○, 8 keV(Cu tube) and Δ, 4 keV (synchrotron radiation).

($FWHM_G[4\ keV] = 0.22°$. A similar effect was observed for harder radiation, which indicates that there is a redistribution of radiation scattered inside the channels of the capillary system. The obtained discrepancy of the results can be explained by the wave nature of the scattering of X-ray radiation in capillary structures. The last fact is just one more confirmation that the geometrical (ray) approximation, while being a valuable tool for estimating the effectiveness of radiation transmission through capillaries, in the description of the process of radiation transmission through a capillary system may lead to serious mistakes in calculations of the angular and spatial characteristics of the radiation.

What is interesting is that these special features of the propagation of radiation in capillaries were also discovered in experiments on the deflection of beams of thermal neutrons ($\lambda \simeq 5$ Å) by special benders (Fig. 19) [122, 123]. The experimentally measured dependence of the intensity of a neutron beam after transmission through a bent system of polycapillaries clearly exhibits a change in the curve's gradient: up to deflection angles of about 10° there is a sharp drop in the effectiveness of transmission, but after that there is only a slow decrease in the number of neutrons at the exit of the optical system with an increasing bending angle. Such behavior cannot be explained by the characteristics of the bender; neither can it be explained if we remain in the framework of geometrical (ray) optics. A possible explanation is presented by the fact that in the transmission of radiation through bent channels of polycapillaries, part of the beam (even if a very insignificant part) undergoes coupled propagation along the inner surface of the channels (which is explained by wave mechanics) and is capable of remaining in the channeling mode even if the polycapillaries are significantly bent, while the main part of the radiation propagates along the channels, is reflected by the walls according to the laws of geometrical optics, and is more susceptible to 'dechanneling' (when the grazing angles exceed the Fresnel angle). The latter fraction is predominant in the overall flux of the radiation in a polycapillary, and this manifests itself at small reflection angles. It is because of the difference in the rates of dechanneling of these parts of the radiation that this effect can be observed when the bending angle is increased. The validity of such an interpretation is corroborated by the theoretical work on the quantum mechanical description of the process of propagation of a neutron beam in the channels of capillary systems [124, 125].

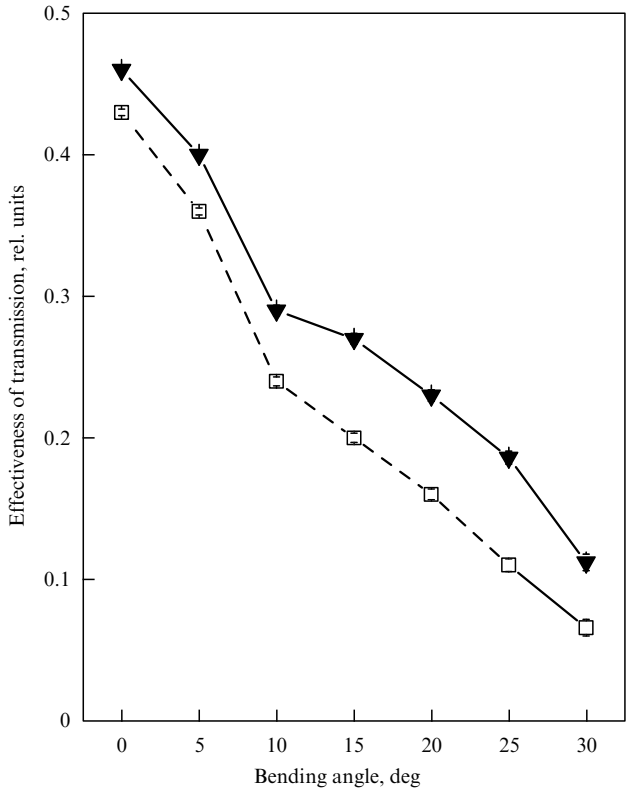

Figure 19. Effectiveness of the deflection of a beam of thermal neutrons ($\lambda \simeq 5$ Å) by a polycapillary (60 capillaries) bender ($150 \times 30 \times 0.5$ mm) as a function of the system's bending angle without a filter (□) and with a Be filter (▼).

8. Applications of capillary optics

The rapid development of X-ray optics has produced many problems for physicists. These problems are related to the possibility of focusing radiation and increasing the concentration of fluxes of neutral particles. The unavoidable energy losses that accompany the widely known methods of controlling beams of X-ray photons have made it essential to seek new ways of forming beams of neutral particles.

One outcome of the intensive research was the creation in the middle of the 1980s of X-ray polycapillary optics. The main principle underlying the new optics consisted in the high effectiveness of the reflection of X-rays in grazing incidence onto a material surface. The proposed controlling device was a system of hollow glass capillaries in which the X-ray photons would be transmitted (as in channels) via multiple TER.

In the last 15 years X-ray capillary optics evolved from an attractive and simple idea into an independent area in optics that is being actively developed. A technology for fabricating monocapillaries and polycapillaries (and also composite and solid-drawn capillary systems) was created and is currently being perfected (so far there have been four generations of capillary lenses). In contrast to the ordinary methods of focusing X-ray radiation, the new capillary optics makes it possible to really handle beams of X-rays. Capillary lenses allow one to focus radiation, to transform a diverging beam of photons into a quasiparallel beam or to compress a parallel beam, to filter radiation by wavelength, etc. [126–136].

The problem of cutting off the hard part of electromagnetic radiation plays an important role in radiation physics. Filtration of the hard part of the spectrum of X-ray radiation can be achieved by using capillary systems. The mechanism of filtration is related to the fact that a photon propagates inside channels via multiple reflection from the walls, provided that the grazing angle is small ($\theta \leqslant \theta_c$). Since the critical TER angle is $\theta_c \propto \omega^{-1}$ (here ω is the photon energy), by selecting a proper geometry of the system we can ensure that for the high-energy part of the beam of photons the condition for channeling (i.e., propagation inside the channel) will not be met, so that this part of the beam will be cut off. But since the single-reflection coefficient in the case of a fixed grazing angle decreases with increasing photon energy, under multiple reflection the hard part of the radiation will, naturally, again be suppressed. Using the same principle, we can monochromatize a polychromatic beam of radiation [110].

Another important property of capillary optical elements is the theoretical possibility of producing optical devices with a large aperture ratio compared to other optical devices of the X-ray range, which would make it possible to use capillary

systems to transfer information and images and also to build an X-ray microscope with a high resolution and a high radiation density.

The potential of capillary optics in X-ray lithography must also be mentioned. The use of capillary systems will make it possible to generate high-power wide beams of X-ray photons with very small divergence angles ($\sim \theta_c$) and also to build high-power sources of soft X-ray radiation for lithography [110].

Another important potential field of application stems from the possibility of suppressing scattered radiation by using capillary systems and of diminishing the irradiation doses without degradation of the parameters being investigated [110, 137, 138].

Obviously, X-ray capillary optics can be used in many areas where it is necessary to increase the density of X-rays and, in general, to monitor the level of X-ray radiation (see the special issues devoted to capillary optical systems [139, 140]). Below we list only the main areas:

— the creation of a new class of medical apparatus (devices used in mammography and angiography) for early detection of cancer and cardiologic disorders: the use of capillary systems would reduce the radiation dose by a factor of several hundred and it would become possible to detect a cancerous growth of about 100 μm in diameter or even smaller [110, 137 – 142];

— the creation of new types of microscopes and tomographs with a resolution of about 0.1 μm for biology and related areas of research [143];

— the creation of devices for elemental microanalysis (with a recording limit of about $\sim 10^{-13}$ g), transferring images, studying crystals, and perfecting diffractometers: the sensitivity of devices and the rate at which information can be gathered will increase by a factor of several dozen [110, 143 – 151];

— the development of X-ray lithography for the fabrication of integrated circuits with a resolution of about 0.1 – 0.2 μm;

— the designing of new X-ray sources with a power of about 10 W and with an effective focal spot smaller than 20 μm (radiation pulses of about 10^{13} phot s^{-1}, which corresponds to an integrated intensity of about 10^7 – 10^8 phot s^{-1});

— X-ray astronomy: it becomes possible to build new types of telescopes in the X-ray range, etc. [143].

Synchrotrons are known to be the strongest sources of quasiparallel X-ray radiation [152, 153]. The average density of synchrotron radiation generated by modern storage rings may reach values as high as 10 W cm^{-2}. The use of capillary optical structures makes it possible to increase the density of the radiation flux by a factor of several dozen to several hundred, which boosts the potential of using synchrotron radiation in problems of spectroscopy and diffractometry [154 – 161].

The possibility of controlling beams of thermal neutrons by capillary systems is also of great interest. This idea was implemented in the early 1990s in the first neutron capillary lens [162, 163]. Since then, research has been conducted in France, Germany, Russia, and the United States in the field of focusing and deflecting neutron beams. This research has shown that capillary systems fabricated in a certain way are capable of focusing a beam with increased density by a factor greater than 100 and effectively (25 – 30%) deflecting beams up to 20°, with the systems being only 15 cm long [122, 123].

There is also an entirely new way in which solid-drawn (integral) capillary systems can be used. It happens that capillary systems fabricated in a special way may be of considerable interest as waveguides for not only X-ray radiation but also for light. Recent years have seen intensive research in creating a new type of optical waveguides known as holey fibers (HFs) [167]. By design, X-ray waveguides and HFs are quite similar: both consist of closely packed glass capillaries. There is an important difference, however: while in HFs the radiation propagates in a glass medium (due to the phenomenon of total internal reflection), in X-ray capillary systems the radiation is transmitted through the hollow sections of the capillaries (the phenomenon of total external reflection). Obviously, in order to be able to transmit radiation the 'transparency' of such systems must be at its maximum; in other words, in X-ray capillary systems the ratio of the area of the hollow channels to the area occupied by the walls between the channels must be as high as possible, while in HFs most often this ratio must be low. This difference determines the requirements of the technology of fabricating capillary structures used in building HFs and X-ray (or neutron) capillary systems. The periodicity in the arrangement of the channels in the transverse plane of the waveguides may lead to interference effects in the transmission of X-ray photons and to single-mode propagation of radiation within a broad optical frequency range. What unites these two types of waveguides is that they make it possible to minimize the losses of radiation power in both frequency ranges considered here.

9. Conclusion

Research in capillary optics has revealed a number of features in the transmission of X-rays through capillary systems. The geometric (ray) optics approximation, often used in calculations of the characteristics of transmission of radiation through capillary systems, can be used only if the number of wave modes is large, so that summation over individual modes can be replaced by integration over angles. The decrease in the power of the radiation transmitted through capillary systems is caused primarily by the absorption of radiation by the walls of the capillary channels. In view of surface channeling of X-ray photons in their motion through capillary channels, coherent scattering may take place at angles smaller than the incidence angles with respect to the channel walls. Here, the angular distribution exhibits a peak in the direction of coherent scattering and broadens because of the diffuse (incoherent) scattering of radiation on the surface roughnesses. The divergence of X-ray radiation behind the capillary systems may be made smaller if there is a certain correlation between the beam parameters and the parameters of the optical system. Thus, in recent years research has shown that capillary systems, while being highly effective in increasing the density of the radiation flux, can be of interest in studies of the processes of scattering of radiation by surfaces of different roughness and curvature.

From the viewpoint of basic research, the transition from capillaries with micron channels to nanotubes, which can be considered nanocapillaries, is a very interesting factor. According to the results of studies conducted in recent years, such a dramatic change in the diameter of the channels leads to a qualitative change in the process of radiation transmission through such structures: while the propagation of radiation in microcapillaries is surface channeling of the photons along the inner wall of a capillary, in nanocapillaries

we are dealing with bulk channeling. The interest in using nanocapillaries in applications is extremely high if only because such systems make it possible to effectively control beams of not only X-ray radiation but also gamma radiation, or beams of not only thermal neutrons but also high-energy neutrons. However, while there is real progress in the fabrication of microcapillary structures and while microcapillary optics is finding more and more applications, the fabrication of nanostructures still has many problems of a purely technological nature to solve.

Today, X-ray optics (and, for that matter, neutron optics) is an independent area of physics undergoing a new stage in its development. This fact can be explained by the close links to modern technology: the apparent decline of interest in studies of this kind, which can be explained by technological difficulties, has been successfully overcome. Lately there has emerged a new area of X-ray optics, capillary optics (often called 'polycapillary optics' in the literature). Capillary optics has for the first time allowed us to really control X-ray radiation within a broad frequency range. The new optics, which differs favorably from other methods of focusing X-ray radiation, makes it possible to monochromatize a beam of radiation, effectively turn it by large angles, transform a divergent beam into a parallel beam and vice versa, and, finally, focus the radiation with the intensity increasing by a factor of 100 to 1000 (or even more). All this has made the list of applied problems in which X-ray optics may produce a real breakthrough only longer. In addition to what we have said above, capillary systems are really new interference elements. The manifestation of the wave properties in such macrostructures is of great interest, since the characteristics of interference may really be controlled. It is also interesting how capillaries and capillary systems can be used as X-ray waveguides. Researchers have focused their attention on X-ray capillary optics primarily because its use promises new applications, both in purely scientific problems and in applied problems. The use of capillary structures has contributed greatly to experiments in diffractometry, in 3D elemental analysis, in controlling beams of synchrotron radiation, in the production of high-power sources of X-ray radiation, and in many other areas. Promising results have been obtained in the use of capillary optics in X-ray lithography, as well as in X-ray imaging techniques. So far these results have been obtained in laboratories, but soon pilot models will be built on their basis. The widest area of research involves applications of the new optics in medicine, in particular in mammography and angiography, and in boron–neutron therapy (capillary optics is a powerful instrument for controlling beams of thermal neutrons). There is hope that research in these areas will produce in the near future new medical devices that will help in the early detection of cancer and cardiologic disorders, and also devices for radiotherapy.

In conclusion, I would like to thank all my colleagues at the High-Energy Electron Laboratory of FIAN (P N Lebedev Physics Institute of the Russian Academy of Sciences), the Institute of Roentgen Optics, and the Laboratori Nazionali di Frascati (Italy), whose active participation in my work made my research, the results of which are presented here, possible. I would also like to note the contribution of M N Yakimenko, whose untimely death saddened us all. He contributed by his studies of the properties of capillary optical elements with the C-60 as the source of synchrotron radiation. I am also grateful to A A Komar and V A Isakov for their useful remarks.

This work was made possible by the support of the Russian Federal Program 'Integration'.

References

1. Röntgen W K *Sitzungsber. Würzburger Phys. Med. Gesellschaft* 1 (1895)
2. Herneck F *Bahnbrecher des Atomzeitalters: Grosse Naturforscher von Maxwell bis Heisenberg* (Berlin: Buchverlag Der Morgen, 1977) [Translated into Russian of an earlier edition (Moscow: Progress, 1974)]
3. Schmahl G , Rudolph D (Eds) *X-Ray Microscopy* (Berlin: Springer, 1984) [Translated into Russian (Moscow: Mir, 1987)]
4. Michette A *Optical Systems for Soft X-Rays* (New York: Plenum Press, 1986) [Translated into Russian (Moscow: Mir, 1989)]
5. Turcu I C E, Dance J B *X-Rays from Laser Plasmas: Generation and Applications* (Chichester: Wiley, 1999)
6. Attwood D T *Soft X-Rays and Extreme Ultraviolet Radiation: Principles and Applications* (Cambridge: Cambridge Univ. Press, 1999)
7. Fridrich W, Knipping P, von Laue M *Sitzungsber. Bayer. Akad. Wiss.* 303 (1912)
8. Compton A H *Philos. Mag.* **45** 1121 (1923)
9. Jentzsch F *Phys. Z.* **30** 268 (1929)
10. Kirkpatrik P, Baez A V *J. Opt. Soc. Am.* **38** 766 (1948)
11. Wolter H *Ann. Phys.* (Leipzig) **10** 286 (1952)
12. Spiller E *Appl. Phys. Lett.* **20** 365 (1972)
13. Rowland H A *Philos. Mag.* **13** 469 (1882)
14. Hutley M C *Diffraction Gratings* (Techniques of Physics, Vol. 6) (London: Academic Press, 1982)
15. Vinogradov A V (Ed.) *Zerkal'naya Rentgenovskaya Optika* (X-ray Optics and Surface Science) (Leningrad: Mashinostroenie, 1989) [Translated into English (Bellingham, Wash.: SPIE, 1995)]
16. James R W *The Optical Principles of the Diffraction of X-rays* (London: Bell, 1948) [Translated into Russian (Moscow: IL, 1950)]
17. Kumakhov M A, Komarov F F *Phys. Rep.* **191** 289 (1990)
18. *McGraw-Hill Yearbook of Science and Technology* Vol. 487 (New York: McGraw-Hill, 1993)
19. Underwood J H, Attwood D T *Phys. Today* **37** (4) 44 (1984) [Translated into Russian: *Usp. Fiz. Nauk* **151** 105 (1987)]
20. Henke B L et al. *Atom. Data Nucl. Data Tables* **27** 1 (1982)
21. Landau L D, Lifshitz E M *Elektrodinamika Sploshnykh Sred* (Electrodynamics of Continuous Media) (Moscow: Nauka, 1982) [Translated into English (Oxford: Pergamon Press, 1984)]
22. Vinogradov A V, Kozhevnikov I V *Tr. Fiz. Inst. Akad. Nauk SSSR* **196** 18 (1989)
23. Riekel C *Rep. Prog. Phys.* **63** 233 (2000)
24. Zimkina T M, Fomichev V A *Ul'tramyagkaya Rentgenovskaya Spektroskopiya* (Ultrasoft X-ray Spectroscopy) (Leningrad: Izd. LGU, 1971)
25. Bass F G, Fuks I M *Wave Scattering from Statistically Rough Surfaces* (New York: Pergamon Press, 1979)
26. Barbee T W (Jr) 'Multilayers for X-ray optics applications', in *X-Ray Microscopy* (Eds G Schmahl, D Rudolph) (Berlin: Springer, 1984) [Translated into Russian (Moscow: Mir, 1987) p. 144]
27. Tatchyn R O 'Optimum zone plate theory and design', in *X-Ray Microscopy* (Eds G Schmahl, D Rudolph) (Berlin: Springer, 1984) [Translated into Russian (Moscow: Mir, 1987) p. 40]
28. Snigirev A et al. *Nature* **384** 49 (1996)
29. Lengeler B et al. *J. Appl. Phys.* **84** 5855 (1998)
30. Lengeler B et al. *Appl. Phys. Lett.* **74** 3924 (1999)
31. Piestrup M A et al. *Nucl. Instrum. Meth. B* **173** 170 (2001)
32. Pearlman J S, Benjamin R F *Appl. Opt.* **16** 94 (1977)
33. Plotkin M E, Slemzin V A, Preprint No. 123 (Moscow: P N Lebedev Physics Institute, 1985)
34. Vinogradov A V, Zorev N N, Kozhevnikov I V "O predel'hykh vozmozhnostyakh optiki myagkogo rentgenovskogo diapazona" ("On the limits of optics of the soft X-ray range"), in *Klassicheskie i Kvantovye Effekty v Elektrodinamike* (Classical and Quantum Effects in Electrodynamics) (Proc. (Trudy) P N Lebedev Physics Institute, Vol. 176, Ed. A A Komar) (Moscow: Nauka, 1986)
35. Kumakhov M A *Nucl. Instrum. Meth. B* **48** 283 (1990)
36. Hirsch P B, Kellar J *Proc. Phys. Soc. London Ser. B* **64** 369 (1951)

37. Pound E, Rebka C *Phys. Rev. Lett.* **3** 439 (1959)
38. Mamontov E A *Zavod. Lab.* **26** 496 (1960)
39. Marton J *Appl. Phys. Lett.* **9** 194 (1966)
40. Mallozzi F et al. *J. Appl. Phys.* **45** 1891 (1974)
41. Anan'in O et al., Inventors' certificate USSR No. 520863 (1974); *Byull. Izobret.* (11) 229 (1974)
42. Mosher D, Stephanakis S *Appl. Phys. Lett.* **29** 105 (1976)
43. Kumakhov M A, Inventors' certificate USSR No. 1322888 (1984)
44. Kumakhov M A *Izluchenie Kanalirovannykh Chastits v Kristallakh* (Radiation from Channeled Particles in Crystals) (Moscow: Énergoatomizdat, 1986); see also Kumakhov M A, Komarov F F *Radiation from Charged Particles in Solids* (Ed. E P Velikhov) (New York: AIP, 1989)
45. Vinogradov A V et al. *Zh. Tekh. Fiz.* **55** 244 (1985) [*Sov. Phys. Tech. Phys.* **30** 145 (1985)]
46. Vinogradov A V et al. *Zh. Tekh. Fiz.* **55** 567 (1985) [*Sov. Phys. Tech. Phys.* **30** 335 (1985)]
47. Komarov F F et al. *Poverkhnost* (6) 31 (1986) [*Phys., Chem., Mech. of Surfaces* **5** 1360 (1990)]
48. Stern E A et al. *Appl. Opt.* **27** 5135 (1988)
49. Engström P et al. *Nucl. Instrum. Meth. A* **302** 547 (1991)
50. Thiel D J et al. *Nucl. Instrum. Meth. A* **317** 597 (1992)
51. Marcuse D *Theory of Dielectrical Optical Waveguides* (New York: Academic Press, 1964)
52. Dabagov S B et al. *J. Synchrotron Radiat.* **2** 132 (1995)
53. Dabagov S B et al. *Nucl. Instrum. Meth. B* **108** 213 (1996)
54. Tatarskii V I *Wave Propagation in a Turbulent Medium* (New York: McGraw-Hill, 1961)
55. Dabagov S B et al. *Proc. SPIE* **3444** 486 (1998)
56. Dabagov S B et al. *Appl. Opt.* **39** 3338 (2000)
57. Bogolyubov N N, Mitropol'skiĭ Yu A *Asimptoticheskie Metody v Teorii Nelineĭnykh Kolebaniĭ* (Asymptotic Methods in the Theory of Nonlinear Oscillations) (Moscow: Nauka, 1958) [Translated into English (New York: Gordon and Breach, 1962)]
58. Landau L D, Lifshitz E M *Mekhanika* (Mechanics) (Moscow: Nauka, 1973) [Translated into English (Oxford: Pergamon Press, 1976)]
59. Babich V M, Buldyrev V S *Asimptoticheskie Metody v Zadachakh Difraktsii Korotkikh Voln. Metod Etalonnykh Zadach* (Short-Wavelength Diffraction Theory: Asymptotic Methods) (Moscow: Nauka, 1972) [Translated into English (Berlin: Springer, 1991)]
60. Yakovlev G D *Tablitsy Funktsiĭ Eĭri* (Tables of Airy Functions) (Moscow: Nauka, 1969)
61. Abramowitz M, Stegun I A (Eds) *Handbook of Mathematical Functions with Formulas, Graphs, and Mathematical Tables* (New York: Dover, 1964) [Translated into Russian (Moscow: Nauka, 1979)]
62. Glauber R J *Phys. Rev.* **131** 2766 (1963)
63. Dabagov S B et al. *Proc. SPIE* **3444** 486 (1998)
64. Alexandrov Yu M et al. *Nucl. Instrum. Meth. B* **134** 174 (1998)
65. Cappuccio G et al. *Appl. Phys. Lett.* **78** 2822 (2001)
66. Kimball J C, Bittel D *J. Appl. Phys.* **74** 877 (1993)
67. Cappuccio G, Dabagov S B *Proc. SPIE* **4138** 88 (2000)
68. Compton A H, Allison S K *X-rays in Theory and Experiment* (New York: D. Van Nostrand Co., 1935)
69. Dabagov S B, Kumakhov M A *Proc. SPIE* **2515** 124 (1995)
70. Dabagov S B, Ognev L I *Zh. Tekh. Fiz.* **58** 1695 (1988) [*Sov. Phys. Tech. Phys.* **33** 1025 (1988)]
71. Dabagov S B, Ognev L I *Nucl. Instrum. Meth. B* **30** 185 (1988)
72. Dabagov S B, Ognev L I *Zh. Tekh. Fiz.* **58** 256 (1988) [*Sov. Phys. Tekh. Phys.* **33** 158 (1988)]
73. Fleck J A (Jr), Morris J R, Feit M D *Appl. Phys.* **10** 129 (1976)
74. Sziklas E A, Siegman A E *Appl. Opt.* **14** 1874 (1975)
75. Arkad'ev V A et al. *Usp. Fiz. Nauk* **157** 493 (1989) [*Sov. Phys. Usp.* **32** 271 (1989)]
76. Kumakhov M A et al., Preprint IROS-1/94 (Moscow: IROS, 1994)
77. Lindhard J *K. Dan. Vidensk. Selsk. Mat.-Fys. Medd.* **34** (14) (1965) [Translated into Russian: *Usp. Fiz. Nauk* **99** 249 (1969)]
78. Thompson M W *Contemp. Phys.* **9** 375 (1968)
79. Gemmell D S *Rev. Mod. Phys.* **46** 129 (1974)
80. Dabagov S B, Kumakhov M A, Nikitina S V *Phys. Lett. A* **203** 279 (1995)
81. Artemiev N et al. *Phys. Scripta* **57** 228 (1998)
82. Dabagov S B, Marcelli A *Appl. Opt.* **38** 7494 (1999)
83. Kukhlevsky S V et al. *Nucl. Instrum. Meth. B* **168** 276 (2000)
84. Dabagov S B, in *X-ray and Inner-Shell Processes* (AIP Conf., Proc., Vol. 652, Eds A Bianconi, A Marcelli, N L Saini) (Melville, NY: American Institute of Physics, 2003) p. 89
85. Dabagov S B et al. *Nucl. Instrum. Meth. B* **187** 169 (2002)
86. Dabagov S B et al. *Proc. SPIE* **4138** 79 (2000)
87. Dabagov S B, in *Otchet NIR FIROS* (Scienific Report of the Institute for Röntgen Optical Systems) (Nalchik – Moscow: FIROS, 1992)
88. Chien Liu, Golovchenko J A *Phys. Rev. Lett.* **79** 788 (1997)
89. Spiller E, Segmüller A *Appl. Phys. Lett.* **24** 60 (1974)
90. Smith N V, Howells M R *Nucl. Instrum. Meth. A* **347** 115 (1994)
91. Nasonov N N *Pis'ma Zh. Tekh. Fiz.* **5** 982 (1979)
92. Zhevhago N K, Ryazanov M I *Fiz. Tverd. Tela* **28** 130 (1986) [*Sov. Phys. Solid State* **28** 70 (1986)]
93. Vysotskiĭ V I, Kuz'min R N *Zh. Eksp. Teor. Fiz.* **94** (8) 351 (1988) [*Sov. Phys. JETP* **67** 1715 (1988)]
94. Zhevhago N K, Glebov V I *Zh. Eksp. Teor. Fiz.* **118** 579 (2000) [*JETP* **91** 504 (2000)]
95. Kumakhov M A *Proc. SPIE* **4155** 2 (2000)
96. Saito R, Dresselhaus G, Dresselhaus M S *Physical Properties of Carbon Nanotubes* (London: Imperial College Press, 1998)
97. Burattini E, Dabagov S B *Nuovo Cimento B* **116** 361 (2001)
98. Burattini E, Dabagov S B, Monti F *Nuovo Cimento B* **117** 769 (2002)
99. Iijima S *Nature* **354** 56 (1991)
100. Ajayan P M, Iijima S *Nature* **361** 333 (1993)
101. Iijima S, Ichihashi T *Nature* **363** 603 (1993)
102. Zhevago N K, Glebov V I *Phys. Lett. A* **250** 360 (1998)
103. Dedkov G V *Nucl. Instrum. Meth. B* **143** 584 (1998)
104. Klimov V V, Letokhov V S *Phys. Lett. A* **222** 424 (1996)
105. Klimov V V, Letokhov V S *Phys. Lett. A* **226** 244 (1997)
106. Bellucci S et al. *Nucl. Instrum. Meth. B* **202** 236 (2003); physics/0208081
107. Biryukov V M, Bellucci S *Phys. Lett. B* **542** 111 (2002)
108. Yablanovitch E *Phys. Rev. Lett.* **58** 2059 (1987)
109. Fayazov R F et al., Preprint IAE-5432/14 (Moscow: IAE, 1991)
110. Kumakhov M A (Ed.) *Optics of Beams* (Moscow: IROS, 1993)
111. Bilderback D H, Hoffman S A, Thiel D J *Synch. Rad. News* **7** 27 (1994)
112. Ullrich J B et al. *Nucl. Instrum. Meth. A* **347** 401 (1994)
113. Welnak C, Chen G J, Cerrina F *Nucl. Instrum. Meth. A* **347** 344 (1994)
114. Kulikov O F *Tr. Fiz. Inst. Akad. Nauk SSSR* **80** 3 (1975)
115. Aleksandrov Yu M et al., Preprint No. 71 (Moscow: P N Lebedev Physics Institute, 1988)
116. Nikitina S V et al. *Proc. SPIE* **2278** 191 (1994)
117. Aleksandrov Yu M, Yakimenko M N *Nucl. Instrum. Meth. A* **359** 12 (1995)
118. Dabagov S B et al. *Proc. SPIE* **2515** 506 (1995)
119. Vincze L et al. *X-ray Spectrom.* **24** 27 (1995)
120. Kukhlevsky S V, Kozma L, Negrea K *J. Mod. Opt.* **43** 2595 (1996)
121. Kukhlevsky S V et al. *Appl. Opt.* **39** 1059 (2000)
122. Ioffe A, Dabagov S B, Kumakhov M A *Neutron News* **6** 20 (1995)
123. Dabagov S B, Marcelli A, Kumakhov M A *Proc. SPIE* **4155** 86 (2000)
124. Calvo M L *J. Phys. D: Appl. Phys.* **33** 1666 (2000)
125. Rohwedder B *Phys. Rev. A* **65** 043619 (2002)
126. Filimonov A G et al., Preprint IAE-5430/11 (Moscow: IAE, 1991)
127. Arkad'ev V A, Kumakhov M A, Fayazov R F, in *Tezisy Dokladov 3-ĭ Vsesoyuznoĭ Konf. po Izlucheniyu Rel. Chast. Kristallov* (Abstracts 3rd All-Union Conf. on Emission by Rel. Particles in Crystals) (Nalchik, 1988) p. 185
128. Filimonov A G et al., Preprint IAE-5431/11 (Moscow: IAE, 1991)
129. Dzhangobegov R P, in *Tezisy Dokladov 1-ĭ Vsesoyuznoĭ Konf. po Opt. Obrabotke Informatsii* (Abstracts 1st All-Union Conf. on Opt. Information Processing) (Leningrad, 1988) p. 123
130. Fayazov R F, Kumakhov M A, in *Abstr. IV All-Union Conf. on Intern. of Rad. with Solids* (Moscow – Nalchik, 1990) p. 94
131. Kovantsev V E et al., in *Abstr. IV All-Union Conf. on Intern. of Rad. with Solids* (Moscow – Nalchik, 1990) p. 97
132. Bukreev S S, Kumakhov M A, Ponomarev I Yu, in *Abstr. IV All-Union Conf. on Intern. of Rad. with Solids* (Moscow – Nalchik, 1990) p. 99

133. Furuta K et al. *Rev. Sci. Instrum.* **64** 135 (1993)
134. Lei Wang et al. *J. Appl. Phys.* **80** 3628 (1996)
135. Chen G-J et al. *Nucl. Instrum. Meth. A* **347** 407 (1994)
136. Ullrich J B, Kovantsev V E, MacDonald C A *J. Appl. Phys.* **74** 5933 (1993)
137. Kumakhov M A, Shovkun V Ya, Preprint IAE-5418/14 (Moscow: IAE, 1991)
138. Nikitin A N et al. *Proc. SPIE* **2519** 165 (1995)
139. Kumakhov M A (Ed.) *Kumakhov Optics and Applications*: *Selected Research Papers on Kumakhov Optics and Application 1998 – 2000* (Proc. SPIE, Vol. 4155) (Bellingham, Wash.: SPIE, 2000)
140. Revenko A G, Dabagov S B *Zavod. Lab.* **68** (5) 3 (2002)
141. Beloshitsky V V et al., Preprint IAE-5707/14 (Moscow: IAE, 1994)
142. Poturaev S V et al., Preprint IAE-5413 /14 (Moscow: IAE, 1991)
143. *Institute for Röntgen Optical Systems* (Moscow: IROS, 1994)
144. Kovantsev V E et al. *Appl. Phys. Lett.* **62** 2905 (1993)
145. Pantojas V M et al. *Nucl. Instrum. Meth. A* **333** 607 (1993)
146. MacDonald C A *J. X-ray Sci. Technol.* **6** 32 (1996)
147. Yamamoto N, Hosokawa Y *Jpn. J. Appl. Phys. Pt. 2* **27** L2203 (1988)
148. Yiming Y, Xunliang D *Nucl. Instrum. Meth. B* **82** 121 (1993)
149. Attaelmanan A et al. *Rev. Sci. Instrum.* **66** 24 (1995)
150. Kantsyrev V L et al. *J. X-ray Sci. Technol.* **7** 139 (1997)
151. Nikitina S V, Scherbakov A S, Ibraimov N S *Rev. Sci. Instrum.* **70** 1 (1999)
152. Sokolov A A, Ternov I M (Eds) *Sinkhrotronnoe Izluchenie* (Synchrotron Radiation) (Moscow: Nauka, 1966)
153. Krinsky S, Perlman M L, Watson R E, in *Handbook on Synchrotron Radiation* Vol. 1 (Ed. E-E Koch) (Amsterdam: North-Holland, 1983) p. 65
154. Engström P et al. *Nucl. Instrum. Meth. B* **36** 222 (1989)
155. Hoffman S A, Thiel D J, Bilderback D H *Opt. Eng.* **33** 303 (1994)
156. Voss K F et al. *Nucl. Instrum. Meth. A* **347** 390 (1994)
157. Bilderback D H, Hoffman S A, Thiel D J *Science* **263** 201 (1994)
158. Sutton S R et al. *Chem. Geology* **208** 129 (1995)
159. Bilderback D H et al. *J. Synch. Rad.* **1** 37 (1994)
160. Li P-W, Bi R C *J. Appl. Cryst.* **31** 806 (1998)
161. Makhov V N et al. *Synch. Rad. News* **13** 20 (2000)
162. Kumakhov M A, Panin Yu N, Sharov V A *Pis'ma Zh. Tekh. Fiz.* **16** (10) 24 (1990) [*Sov. Tech. Phys. Lett.* **16** 371 (1990)]
163. Kumakhov M A, Sharov V A *Nature* **357** 390 (1992)
164. Mildner D F R, Chen H *J. Appl. Cryst.* **27** 316 (1994)
165. Podurets K M, Sharov V A, Mildner D F R *Appl. Phys. Lett.* **71** 3168 (1997)
166. Podurets K M, Mildner D F R, Sharov V A *Rev. Sci. Instrum.* **69** 3541 (1998)
167. Zheltikov A M *Usp. Fiz. Nauk* **170** 1203 (2000) [*Phys. Usp.* **43** 1125 (2000)]